








# Comparative analysis of manual and digital approaches for extracting geological hiatuses. A case study from China<sup>☆,☆☆</sup>

Berta Vilacís<sup>a,\*,</sup>, Sara Carena<sup>a,</sup>, Jorge N. Hayek<sup>a,</sup>, Gabriel Robl<sup>a,</sup>, Hans-Peter Bunge<sup>a</sup>, Jincheng Ma<sup>b,</sup>

<sup>a</sup> Department of Earth and Environmental Sciences, Ludwig-Maximilians-Universität München, Theresienstr. 41 and Luisenstr. 37, Munich, 80333, Germany

<sup>b</sup> School of Earth and Space Sciences, Peking University, No. 5 Yiheyuan Road, Beijing, 100871, China

## ARTICLE INFO

### Keywords:

Hiatus  
Sedimentology  
Unconformity  
Dynamic topography

## ABSTRACT

Dynamic topography is a crucial geodynamic observable that emerges as a consequence of flow in the mantle. Buoyancies associated with mantle convection induce vertical deflections at the Earth's surface. Negative surface deflections create depositional environments and allow sedimentation to occur, while positive surface deflections create erosional/non-depositional environments, that induce gaps (hiatuses) in the geological record. The temporal and spatial extent of these gaps can be mapped using geological maps and regional studies, thus providing a means of tracking mantle processes through geological time. Here, we compare a manual and digital extraction of hiatus distributions in China. We utilise a manually compiled dataset of un/conformable contacts from a previous publication and compare it to a digital contact extraction using the recently published digital geological map of China. The digital approach is limited to surface data, whereas the manual approach allows the utilisation of subsurface information. We find that the digital approach is substantially faster than the manual extraction. Our results indicate that the optimal methodology combines digital processing with refinement of manual subsurface information. Furthermore, we observe that mapping the absence and presence of a geological series shows very similar results when processed using either approach. The current limitation to a wider application of this approach is the limited availability of digital geological maps. A standardised digital database of geological maps enhanced with subsurface information (i.e., covered geological maps) is necessary to promote the use of geological data within the wider Earth science community, and would increase the opportunities for interdisciplinary collaboration.

## 1. Introduction

Uplift and subsidence due to mantle convection shape the Earth's surface. This convectively maintained topography, termed “dynamic topography” by Hager et al. (1985), leaves traces in the geological record. One of the first usages of geological data to infer dynamic topography variations due to mantle downwellings was carried out by Mitrovica et al. (1989) and Burgess et al. (1997). They used the sedimentary record from the Western Interior Seaway and the cratonic interior of North America to study the subsidence of the continent due to the subduction of the Farallon slab. Shortly after, Gurnis (1998) showed that the downwelling under Australia was responsible for the Cretaceous Eromanga Sea, which was later confirmed by Harrington et al. (2019). Alternatively, Sahagian (1987) studied epeirogenic movements in North America and proposed that these motions can provide

insides into subcontinental mantle dynamics and mantle-lithosphere interactions. Bond (1978b, 1979) linked the continent-scale sediment distribution to the uplift of continental platforms and Bond (1978a) stated that Africa experienced a late Tertiary uplift relative to other continents, which agrees with the findings of Burke and Whiteman (1973). Several studies (Cox, 1989; Şengör, 2001; Rainbird and Ernst, 2001; Saunders et al., 2007) concluded that hot mantle upwellings, also known as mantle plumes, create a dome-shaped uplift of 1–2 km over a radius of 1000–2000 km that induces changes in continental drainage patterns. This uplift is followed by large-scale magmatism (i.e., flood basalt eruptions) after the arrival of the plume under the lithosphere (Rainbird and Ernst, 2001; Campbell, 2007; Saunders et al., 2007) and the shear flow generated by this hot material in the asthenosphere induces plate motion changes (Stotz et al., 2021; Vilacís et al., 2022).

<sup>☆</sup> This article is part of a Special issue entitled: ‘DRT 2024’ published in Journal of Structural Geology.

<sup>☆☆</sup> This document is the results of the research project funded by the Deutsche Forschungsgemeinschaft (DFG), Germany.

\* Corresponding author.

E-mail address: [B.Vilacis@lmu.de](mailto:B.Vilacis@lmu.de) (B. Vilacís).

In the sedimentary record, dynamic subsidence leaves accommodation space for sedimentation, whereas dynamic uplift, usually caused by hot mantle upwellings, creates non-depositional or erosional environments, that leave sedimentation gaps in time (Barrell, 1917). These gaps, also termed hiatuses, populate the sedimentary record in the form of unconformities (e.g., Miall, 2016). The existence of unconformities in the geological record has long been known (e.g., Suess, 1883; Blackwelder, 1909; Stille, 1924; Levorsen, 1933; Wheeler, 1958; Belousov and Maxwell, 1962; Sloss, 1963, 1992; Vail et al., 1977; Sahagian and Jones, 1993; Şengör, 2003, 2016) and some authors (e.g., Burgess et al., 1997; Şengör, 2016; Friedrich et al., 2018) pointed out the need of physical models for their interpretation. In particular, Friedrich et al. (2018) and Friedrich (2019) proposed a new method for mapping hiatus surfaces as a way to track and study the inter-regional expression of mantle convection through its dynamic topography. This approach introduces an event-based perspective on stratigraphy and is based on the premise that the lack of information (i.e., sedimentary gaps) can be part of a larger signal. In other words, this approach surpasses the regional lack of information, providing a solution to this interpretational challenge by considering these stratigraphic gaps to be part of the positive mantle dynamic signal at the inter-regional scale. However, it is important to note that hiatus surfaces may be formed due to mantle-driven dynamic topography, but they can also be indicative of eustatic changes (Vilacís et al., 2024), erosional or lithospheric processes. Thus it is possible that some of these may coincide with dynamic processes and thereby generate hiatus surfaces at wavelengths that are similar. We used this method to map hiatus distributions in Europe (Vibe et al., 2018b), Africa (Carena et al., 2019), and the Atlantic and Indo-Australian realms (Hayek et al., 2020, 2021; Vilacís et al., 2022) since the Upper Jurassic. In Vilacís et al. (2024), the method was applied to all continents, except Antarctica, and the continental shelves, using a combination of geological maps (both analogue and digital), stratigraphic columns and regional studies. The resulting maps allowed us to link the absence of sedimentary rocks of a geological series at the continental scale to the rise of mantle plumes (e.g., Hayek et al., 2020). We found that there is a hiatus surface appearing 10–20 Myrs before the arrival of the mantle plume under the lithosphere, and this hiatus is frequently followed by extensive volcanism and a plate motion change (Vilacís et al., 2022; Stotz et al., 2023, 2024). We observed also that some inter-regional hiatuses are not associated with subsequent flood basalt eruptions and can presumably be created by plume material spreading laterally in the asthenosphere for 1000s of kilometres (Brown et al., 2022; Vilacís et al., 2024). This was also postulated by Friedrich et al. (2018) and provides a physical mechanism to induce a complex sedimentary record.

In this study, we use the example case of onshore mainland China to compare the manual approach previously employed to map hiatuses in Asia (Vilacís et al., 2024), and the digital processing of the recently available digital geological map of China (Pang et al., 2017). The latter means processing geological information digitally using digital geological maps in a Geographic Information System (GIS) format, characterised by fully vectorial objects with associated attributes. These maps facilitate the digital manipulation of the objects they encapsulate. Contrarily, the manual approach uses non-vectorial forms of data, such as scanned or rasterised geological maps and involves visual interpretation and manual digitisation of features. Evaluating both digital and manual approaches for mapping hiatuses is essential, as extracting this type of data at continental scale is necessary for studying the imprint of mantle signals in the geological record, which has wavelengths of approximately 2000–3000 km (Hayek et al., 2020; Vilacís et al., 2024). It can also be labour-intensive. Consequently, in the current era of increased computation, and the increasing accessibility of digital geological maps, there is an opportunity to streamline the data extraction process and reduce operational time. In this study, we compare the time expended on the pre-processing steps and the hiatus extraction for both manual and digital approaches. We also examine the accuracy and the

types of input data utilised in each method, and the differences that emerge when using different data sets, such as geological maps that have different spatial scales.

We organise this manuscript as follows: In Section 2, we provide a detailed description of the dataset, the study area, and the digital and manual approaches employed. We follow in Section 3 with the results of both approaches, and then extract the un/conformable surfaces (Section 3.1), and calculate the hiatus ratio (Section 3.2). We discuss the results obtained from the manual and digital approaches in Section 4 and conclude in Section 5.

## 2. Material and method

In our earlier publications, we combined a variety of approaches to map the contact between two geological units, as well as the absence and presence of a geological unit (e.g. Friedrich et al., 2018; Vibe et al., 2018b; Carena et al., 2019; Hayek et al., 2020, 2021; Stotz et al., 2024; Vilacís et al., 2022, 2024). In general, where feasible, we employed a digital approach to extract the contacts, primarily utilising digital geological maps. This approach is advantageous as it is less time-consuming, provides a standardisation of the data and does not require any interpretation. However, a manual approach can facilitate a more in-depth study of a specific region and is the only option where there is a lack of digital data. We employed this approach for the cases of Africa, Asia, and Oceania. Recently, the digital geological map of China compiled by Pang et al. (2017) was made available, therefore enabling a comparison between the manual and digital approaches by utilising our manually extracted compilation from Asia and the one by Pang et al. (2017). Furthermore, China is large enough that a comparison would yield meaningful results, even though it is part of the larger Eurasian continent.

In this study, we adopt the global compilation from our previous publication (Vilacís et al., 2024, see Fig. 2). In this data set, the contacts for Asia were compiled manually (see Table 1 from their supplementary material for an extensive reference list). For the equivalent digital approach, we extract the hiatus contacts/points from the geological map of China (Pang et al., 2017) following the same extraction procedure used in Hayek et al. (2020) for the hiatus surfaces in Europe, North America, South America and Australia. The mapping is conducted at the temporal resolution of geological series (Ogg et al., 2016; Cohen et al., 2013), because this is the temporal resolution of the input data. Yet, the mapping can be applied to lower or higher temporal resolutions as well. For a fair comparison, we utilise for the rest of the continents the global compilation from Vilacís et al. (2024, Fig. 2), modifying only those points that are in the mainland continent and fall within the boundaries given by the onshore mainland Chinese geological map (Pang et al., 2017). Moreover, to avoid introducing additional complexities, and to ensure an accurate comparison between the different time series, and the manual and digital extraction, the points are maintained at the extracted contacts at their present-day location.

### 2.1. Mapping technique

There are two mapping options that we have previously used when extracting hiatus information from the geological record. The first option is the “Base of” mapping, where we strictly map the contact between two geological series at the base of a *target* geological series. For that we followed the methodology introduced by Friedrich (2019) and used later by Carena et al. (2019), where a *conformable* contact is defined when the *target* geological series is in contact with the immediately preceding geological series (i.e., *given* series). Contrarily, an *unconformable* contact (i.e., hiatus) is defined when the *target* geological series is not underlain by the preceding *given* geological series, but rather overlies a gap in the stratigraphic record and is in contact with an older geological series. When the *target* geological series is not present in the input data, the resulting maps show no data and thus

they are *blank* in these areas. For an overview of this mapping choice and specific descriptions see [Carena et al. \(2019\)](#) and Fig. 1(d) in [Vilacís et al. \(2024\)](#) and the respective text.

The second mapping option, which is preferred for observations of dynamic topography in geodynamics, maps both the absence and presence of a *given* geological series, resulting in the so-called hiatus maps. This mapping choice is referred to as “hiatus/no hiatus”. Following ([Hayek et al., 2020](#); [Vilacís et al., 2022, 2024](#)), a *hiatus* is defined as an unconformable contact, and represents the absence of a *given* geological series, whereas a *no hiatus* shows the occurrence of such geological series, irrespective of the presence of the *target* geological series. *Blank* in this mapping represents the absence of both the *target* and the *given* geological series in the input data. In [Vilacís et al. \(2024\)](#) (Fig. 1e), there is a conceptual illustration of this mapping choice accompanied by a detailed text description. In this work, we primarily focus on the “Base of” mapping, where we strictly map conformable and unconformable contacts between geological series.

It is important to note that because we are mapping at the temporal resolution of geological series, an unconformity (or hiatus) has a different duration for different series they represent, whereas a conformity always means no time missing. For example, at the Base of Miocene, an unconformity lasts at least ~11 Myrs, because it represents that the Oligocene is missing, while at the Base of Oligocene, the unconformity has to last at least ~22 Myrs. This unconformity or hiatus could be longer if rocks of the Lower Miocene or Lower Oligocene were missing, respectively. At the time resolution of series we are mapping Miocene or Oligocene as a whole, regardless of potential hiatuses identified in the geological stages within those series (see Fig. 3 from [Hayek et al., 2020](#)).

In both approaches, hiatus mapping is conceptually tied to geological contacts, which are inherently linear features. However, for consistency and further processing, we extract point data from these lines. In the manual approach, the density of these points is determined by the mapper, though it follows the geological target contacts in the rasterised geological map. In contrast, the digital approach is based on standardised vector geometries, which allow for point extraction in a more uniform and reproducible way. This conversion involves extracting vertex points from line features without interpolating between the points. Nonetheless, it is important to note that some level of subjectivity is also inherent in how GIS data are compiled, even in standardised datasets. To enhance the comparison between the two approaches, we apply a spatial regularisation to the extracted points when we prepare the dataset for the spherical harmonic expansion, as described in Section 2.4.

## 2.2. Manual extraction

For the manual extraction, as mentioned earlier, we used the previously compiled data set from [Vilacís et al. \(2024\)](#), which followed the manual extraction of the contacts described in [Carena et al. \(2019\)](#). This data set is a compilation of points mapped as conformable or unconformable along contact lines and below sedimentary cover. They originated from a number of sources, which are mainly continental and regional analogue geological maps, but also online geological databases, correlation charts, drill logs, and regional stratigraphic studies from journal articles or book chapters. For China, as for the rest of Asia, we mainly used two analogue geological maps, one at 1:2.500.000 ([Hwang et al., 2008](#)), and the other at 1:5.000.000 ([Ghose et al., 1990](#)) (see the reference table in the supplementary material from [Vilacís et al., 2024](#), for further information). The maps were first georeferenced, followed by manually mapping the conformity or unconformity at the base contact of each series, from large to small spatial scale. In the case that the data pertains to a sedimentary basin, we ensured that the spatial extent of the basin was adequately covered in accordance with the studies conducted in that region and the spatial resolution of the data available. It should be noted that this approach can introduce

subsurface information into the maps (e.g., stratigraphic columns, drill cores, seismic profiles), thereby extending the coverage of geological maps to include areas that would not otherwise be included, particularly, when a basin is covered by young sediments which overlay older ones. Additionally, it is possible that some subjective interpretation is necessary when mapping the contacts that are not visible at the surface, and they need to be inferred. This is only possible to do in the manual approach.

The time resolution of the geological maps or the regional studies we used is not purely that of geological series, sometimes it is given by a combination of geological series: systems or even larger time intervals. Thus in this approach, we assumed that when the age of a rock unit was given in terms of a geological system, the inner series of that system are present, an assumption which always leads to the mapping of conformable contacts for all the series within that system.

## 2.3. Digital extraction

In the digital approach, we use the 1:1,000,000 geological map database of China ([Pang et al., 2017](#)), which has recently been made available digitally. It consists of 64 sub-databases (in accordance with the international standard division range), and contains stratigraphic rock units, faults, isotopic age data, grids, and other relevant information. We only use the “GEOLOGY” and “GRID” vectorial files for the purpose of this study. This approach utilises a digital geological map made of polygons, from which the contacts between the polygons are extracted recursively for all available time units. The steps undertaken to prepare the “GEOLOGY” files and the extraction of conformable and unconformable data points or the absence and presence of a geological series are described briefly in the following paragraph, and in detail in [Appendix A](#).

The first step is to transform the downloaded data into a format that can be read by either QGIS or ARCGIS. The original files are in MapGIS format, which is a Geographic Information System (GIS) file type specific to the MapGIS software, mainly available in China. We employed MapGIS for the initial conversion of the files to a *shapefile* format. The second step is to reproject each of the 64 sub-databases. This is necessary because the original shapefiles have a local, arbitrary coordinate system. This arbitrary coordinate system complicates the processing, mainly because the reference coordinate system they use is not in the western databases. This step is specific for the case of China, but it is possible that other digital geological maps present other issues and thus need another specific tailored approach to prepare the data, as there is no worldwide standard yet for such maps. For more information on how we reprojected the individual maps, see [Appendix A.1](#).

Once the 64 sub-databases are joined together and saved in a *shapefile*, we create a dictionary that maps the age description of each polygon to a upper (younger) and lower (older) numerical age boundary. This step must be tailored to each specific geological map because there is not yet a common format for describing the geological age of a given polygon. Some agencies use numerical codes, others use name descriptions, and the language varies from agency to agency. A more accurate description on the dictionary can be found in [Appendix A.2](#).

Finally, using the digital geological map (*shapefile*) and the age dictionary, we implement the *Python* program used in our previous publications (e.g., [Hayek et al., 2020](#)). The program is used to extract the geological contacts between the polygons and to classify them as positive (indicating an unconformity and thus a hiatus) or negative (indicating a conformable contact). We also employed a variation of this program to extract the presence or absence of a geological series, when using the “hiatus/no hiatus” mapping. As said before, in this manuscript we primarily focus on the former (“Base of”) mapping technique and extract contacts strictly at the base of a *target* geological series. In the case of China, the preprocessed digital geological map has a size of 200.8MB and contains 105922 polygons. The software



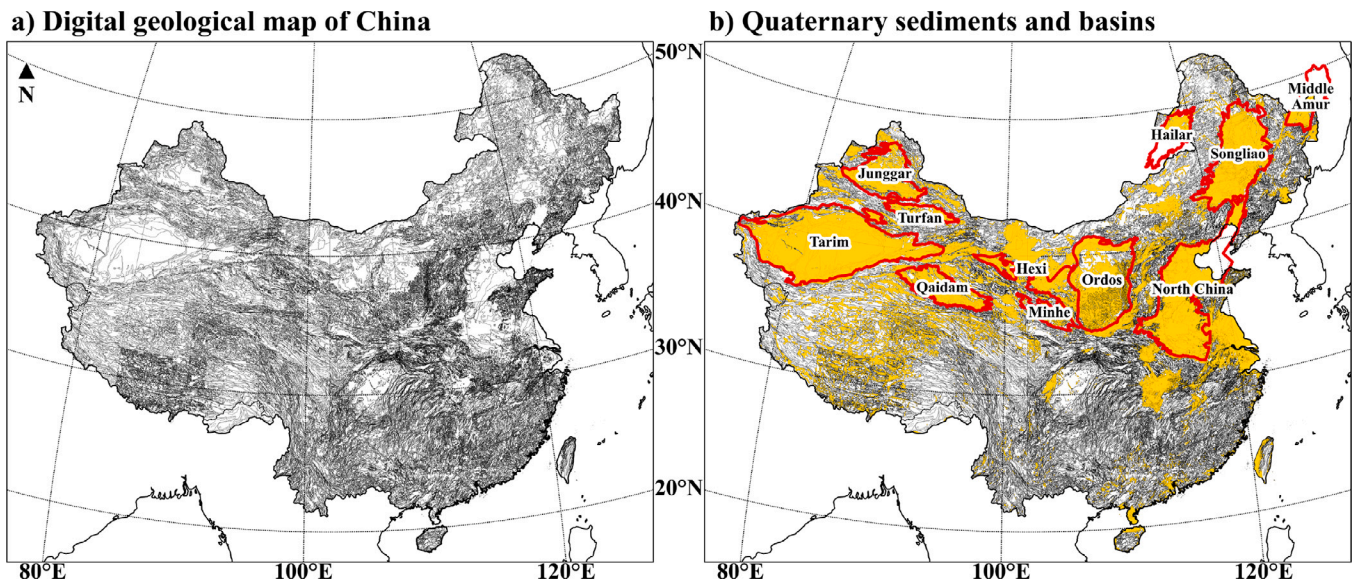


**Fig. 1.** (a) Digital geological map of China after preprocessing. Each polygon, that creates this digital map, represents a geological unit with a given age, formation and lithology and is contoured with a black line. (b) Digital geological map of China with the Quaternary sediments highlighted in yellow. Outlined in red are the main sedimentary basins: Tarim, Junggar, Turfan, Qaidam, Minhe, Hexi, Songliao, North China, Hailar, Ordos and Middle Amur Basins, as defined by CCG-Robertson (2022). In these basins subsurface information was used in the manual approach. The maps use an orthographic projection with the central latitude being 35 degrees North and the central longitude of 102 degrees East. We delimit the plot using the extent feature in cartopy at longitude 77 to 127 and latitudes 16 to 54. That gives the corner coordinates of the maps (lon, lat) as lower-left (77.17, 14.66), lower-right (126.83, 14.66), upper-left (62.00, 50.80) and upper-right (142.00, 50.80).

requires approximately 9 h (8 h and 45 min) to process and extract the contacts from the preprocessed geological map (see Fig. 1a) using just one core on a local computer at LMU-Geophysics (Fujitsu computer with 12 Intel Core i5-10400 CPUs 2.90 GHz and 32 GiB of memory). The software, which also allows for a parallelised extraction, takes 30–45 min using 50 cores on the LMU-Geophysics local cluster (see Oeser et al., 2006; Oeser, 2009, for the specifics). It is important to note that the geological map, similar to the data compiled in the manual approach, has a combination of geological series, systems or even larger time intervals. The age of a polygon is defined by an lower and upper age bound. Consequently, when the age of a polygon is defined by a geological system, only the age bounds associated with that system are mapped. This implies that the contacts defined by the series within that system are not mapped, when using the digital hiatus extraction method.

Fig. 1(a) shows the pre-processed digital geological map of China, while Fig. 1(b) outlines the sedimentary basins in China used in our manual mapping (red), which contain subsurface information in the maps. They are delimited together with the Quaternary sediments from the digital geological map (yellow) for comparison.

#### 2.4. Spherical harmonic expansion

Following the methodology introduced by Hayek et al. (2020), the extracted data points, obtained through either the manual or digital approach, are subsequently subjected to a spherical harmonic expansion. A spherical harmonic expansion is a mathematical way to represent surface patterns on a sphere using a superposition of predefined functions with specific wavelengths and distributions. By weighting each spherical harmonic function with a scaling coefficient appropriate to the amplitudes of the signal, its surface patterns can be approximated with a smooth representation. In this study, we use this expansion to isolate long-wavelength signals and filter out shorter-wavelength features that may arise from local tectonic or erosional processes. This entails the application of a grid regularisation to resample the extracted points to a uniform distribution, which comprises 720 points in latitude and 1440 points in longitude, resulting in a spacing of  $\approx 30$  km between

grid nodes. Each node is assigned a value of +1 (unconformable) or –1 (conformable) depending on the nearest mapped point within half (1/2) of the grid spacing. In the case that no point is within the specified range, the node is assigned to a value of 0. We use the *pyshtools* library (Wieczorek and Meschede, 2018) to perform an expansion up to spherical harmonic degree 100, using fully normalised spherical harmonic coefficients (Stacey and Davis, 2008). Subsequently, we apply a Gaussian taper with a cut-off at degree 15 and a gradual decrease in spectral contribution from degrees 15–60, after which it reaches zero (see Fig. 5 from Hayek et al., 2020). This Gaussian filter is applied to reduce the edge artefacts (Gibbs phenomenon) created when fitting a finite spherical harmonic expansion, which are a result of the binary nature of the data set. This filter preserves wavelengths longer than approximately 1000 km, because our objective is to extract the long-wavelength hiatus signal resulting from mantle dynamic processes. However, we note that mantle signals can occur across a range of wavelengths, and plate flexural effects may start to influence at spherical harmonic degree 33 ( $\sim 1200$  km) (Watts and Moore, 2017), as also revealed by studies of residual topography (e.g., Holdt et al., 2022). For context, China has dimensions of approximately 5250 km from east to west and 5500 km from north to south. Consequently, changes in hiatus surfaces within China will be reflected in the spherical harmonics expansion. In simple words, the spherical harmonic expansion acts as a smoothing tool, reducing local noise and highlights inter-regional to continental scale patterns in conformable and unconformable surfaces. As previously mentioned, we use the global data set from Vilacís et al. (2024), with only those points falling within the Chinese political boundary undergoing modification. This is done to ensure that the changes observed in the resulting spherical harmonic surfaces and hiatus ratios are solely attributable to the two different approaches.

#### 2.5. Hiatus ratio

The hiatus ratio is calculated as the hiatus (unconformable) surface area relative to the combined unconformable and conformable areas of



the target region, in accordance with the definition provided by Hayek et al. (2020) and Eq. (1).

$$HiatusRatio = \frac{Area_{unconf}}{Area_{conf} + Area_{unconf}} \quad (1)$$

where  $Area_{unconf}$  and  $Area_{conf}$  are the sizes of the unconformable and conformable area, respectively. The target region for this work is the country of China, defined by limits of the Chinese digital geological map. After the spherical harmonic expansion, it is composed of conformable and unconformable area, as well as blank areas, where both the target and immediately older series are not present. We also calculate an uncertainty range on the hiatus ratio curves as previously published in the methodology by Carena et al. (2019) and Vilacís et al. (2024). We quantify two maximum bounds of uncertainty by assigning two end-member cases to the blank areas. The blank areas, as previously stated, are the areas where we do not record any signal, because the *target* geological series is absent in that area (i.e., in Base of Miocene that means that Miocene is not present). Thus, assuming that the *target* geological series was deposited, the two end-member cases we consider are: the sedimentary rocks of the preceding *given* geological series were never deposited during their geological series and thus we have an unconformable contact (or hiatus of the preceding geological series) or they were deposited creating a conformable contact, and potentially later eroded. In other words, we consider the blank surfaces as either unconformable surfaces or conformable surfaces. This choice represents a maxim bound for the uncertainty. These calculations are only performed for the surfaces that are situated within the boundaries of China. Eq. (2) shows the uncertainty of the unconformable/hiatus ratio, as described above,

$$Uncertainty_{unconf} = \frac{Area_{unconf} + Area_{blank}}{Area_{target}} \quad (2)$$

where  $Area_{blank}$  is the area where we do not have information of the target geological series and the immediately preceding one and  $Area_{target} = Area_{conf} + Area_{unconf} + Area_{blank}$ . The same is done for the calculation of the conformable uncertainty.

### 3. Results

In this section, we start by presenting the unconformable and conformable points extracted for each map using the digital and manual approaches (Fig. 2). In general, we observe that both approaches have similar amounts of data points. Yet, the manual approach has a higher proportion of conformable points, while the digital approach is characterised by the presence of mainly unconformable contacts throughout the time range studied. Furthermore, the conformable points in the manual approach are predominantly located within the principal sedimentary basins (highlighted in red in Fig. 1b), whereas in the digital approach, no contacts are present in these regions due to the presence of Quaternary sediments covering older strata (yellow areas in Fig. 1b). The areas covered with Quaternary sediments are not visible on the un/conformable maps, with the exception of the Base of Pleistocene, where the contact with other layers is mainly unconformable. However, a comparison of the location of the unconformable points in both approaches reveals that the points are situated in similar areas, particularly in the northern part of the country (north of 40 degrees latitude), where the manual approach has more points. In the southern part, we observe that the manual approach barely shows any contacts: this is due to the input map scale difference, and it becomes most visible in the south of the country because there are not any basins where data was available. Therefore, in this region, it is a simple map-to-map comparison, of which the manual approach used two geological maps with a coarser spatial scale than the digital approach.

For the manual approach, the individual maps show conformable contacts scattered throughout the country at the Base of Lower Cretaceous (Fig. 2a), with a particular concentration in the Tarim, Qaidam

and Songliao Basins. Unconformable points are located in the Ordos Basin and its surrounding areas. At the Base of Upper Cretaceous (Fig. 2b), we find fewer contacts overall. These are mainly conformable, whereas unconformable contacts are very scarce. Similarly, at the Base of Paleocene (Fig. 2c), the contacts are limited in number and mainly conformable, located in the west of the Tarim Basin, the Junggar and Turfan Basins and in the south-east part of China. At the Base of Eocene (Fig. 2d), we have conformable contacts at the same locations as in the Base of Paleocene. Additionally, unconformable points are located in the Qaidam Basin, the west part of the Hexi Basin and the Songliao and Middle Amur Basins. The Base of Oligocene (Fig. 2e) presents contacts predominantly in the northwest and central regions of China, where both conformable and unconformable points can be observed. The former are situated in the Junggar, Turfan, Qaidam, Hexi and Minhe Basins, as well as in the west of the Tarim Basin. Unconformable points are located in the east of the Tarim Basin in the Qaidam Basin, and in the north of the Ordos Basin. For the Base of Miocene (Fig. 2f), the contacts are distributed in the northern part of the country. The Tarim, Turfan, Qaidam, and Hexi basins exhibit a conformity, whereas south of the Tarim and Qaidam basins display unconformities. These points traverse the country from west to east, leaving unconformable patches of points. The Songliao basin also shows an unconformity. The Base of Pliocene (Fig. 2g), shows a comparable distribution of conformable points to the Base of Miocene. The unconformable points are less prevalent and confined to the vicinity of the Qaidam Basin and between the Hailar and Ordos Basins. Finally, the Base of Pleistocene (Fig. 2h) has the highest density of points, with conformable contacts in the Tarim, Junggar, Qaidam, and North China Basins and unconformable contacts surrounding those basins and covering the central and northern parts of the country.

For the digital approach, the Base of Lower Cretaceous (Fig. 2i), shows a vast majority of unconformable points, with the exception of the north-western corner of the country, where the Tarim Basin is located and no contacts are displayed. The Base of Upper Cretaceous (Fig. 2j), shows a reduction in the number of points in comparison to the previous map, with unconformities observed in the south-west and south-east regions of the country. Similarly to the manual approach, there is a concentration of unconformities along the central-north border between China and Mongolia. The Base of Paleocene (Fig. 2k) reveals almost only unconformable points, with the majority concentrated within the Tibetan region. The Base of Eocene map (Fig. 2l) has a reduction of points compared to the Base of Paleocene, with unconformities occurring in similar regions. At the Base of Oligocene (Fig. 2m), only a limited number of unconformable points are observed in the western region of the country. The Base of Miocene (Fig. 2n) shows an increase in the number of unconformable points, situated in the Tibetan region, in the vicinity of the Minhe and Ordos Basins, and the Erlian Basin. At the Base of Pliocene (Fig. 2o), the contacts are distributed in the west and central part of China, with the majority of points being unconformable. Finally, at the Base of Pleistocene (Fig. 2p), similar to the manual approach, there is the highest density of points. In this case they are unconformable points and cover the majority of the country. Blank areas are present in the major basins: the Tarim, Qaidam, part of the Ordos Basin, the east of the North China Basin, and the Songliao Basin.

#### 3.1. Un/conformable surfaces

Fig. 3 shows the un/conformable surfaces obtained after applying a spherical harmonic expansion to the data set depicted in Fig. 2. Note that the intensity of the colours is merely representative of the density of points and does not possess any physical significance. Fig. 3 emphasises the patterns previously described. It demonstrates that the manual approach yields a higher prevalence of conformable surfaces, whereas the digital approach predominantly is covered with unconformable surfaces. In this subsection, we provide a comparative description for

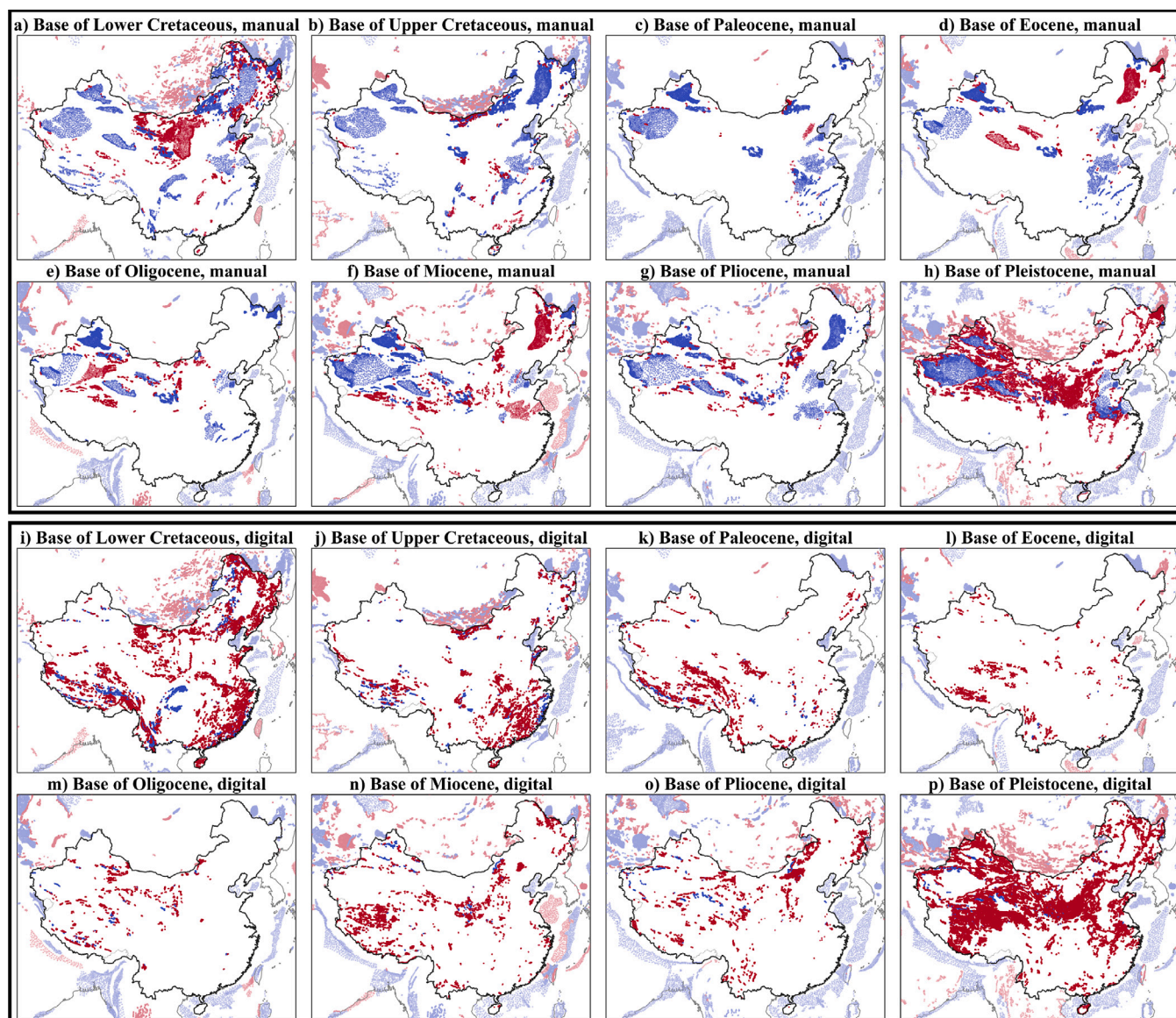


**Fig. 2.** Comparison of manual (upper box) and digital (lower box) extraction of conformable and unconformable contacts. Blue is a conformable contact, and means that there is no time gap and the immediately preceding older geological series is present. Red indicates an unconformable contact, meaning that the immediately preceding older geological series is missing. The points inside the outline of the Chinese geological map are highlighted, while the ones outside have less colour intensity because they remain the same in both approaches. See Fig. 1 for projection and corner coordinates information. Note that the manual approach has a mix of conformable and unconformable points while the digital approach has mainly unconformable contacts (see text).

each geological series, highlighting the differences between the manual and digital approaches.

Overall, the two approaches appear to complement each other. That means, that in the majority of the maps, when a region is covered by both approaches, the surfaces mostly coincide with being either conformable or unconformable. When this is not the case, either one approach has blank areas where the other has the region covered, or both approaches show a blank area in the same place (see Fig. B.1 for a visual comparison).

If we study each geological series, we observe that at the Base of Lower Cretaceous both approaches (Fig. 3a and i) exhibit an unconformable surface in the central-north part of the country (in the Hexi, Ordos and Minhe basins and their surrounding areas), and a conformable surface in the central-south part. In the remaining areas, where at least one of both approaches shows blank surfaces, the manual map displays conformable surfaces, whereas the digital approach shows unconformable surfaces (Fig. B.1). At the Base of Upper

Cretaceous, both maps (Fig. 3b and j) demonstrate a reduction in the extent of un/conformable surfaces. The manual approach encompasses conformable surfaces across the western and eastern regions of China, whereas the digital approach depicts an unconformable surface in south-eastern China. The Base of Paleocene shows a similar conformable coverage for the manual approach (Fig. 3a) as observed in the Base of Upper Cretaceous. In contrast, the digital approach (Fig. 3i) shows an unconformable surface in the south-west region of the country. Once more at the Base of Eocene, the manual approach (Fig. 3d) shows conformable surfaces in the western and south-east part of the country. This approach also depicts unconformable surfaces in the Songliao Basin as well as the east of the Tarim Basin and the Qaidam Basin. To the south of the latter, there is a slight overlap with an unconformable surface in the digital approach (Fig. 3l), that extends further south to the Tibetan area. At the Base of Oligocene, we observe contrasting signals around the Hexi Basin, with the manual approach (Fig. 3e) depicting a conformable surface, whereas the digital



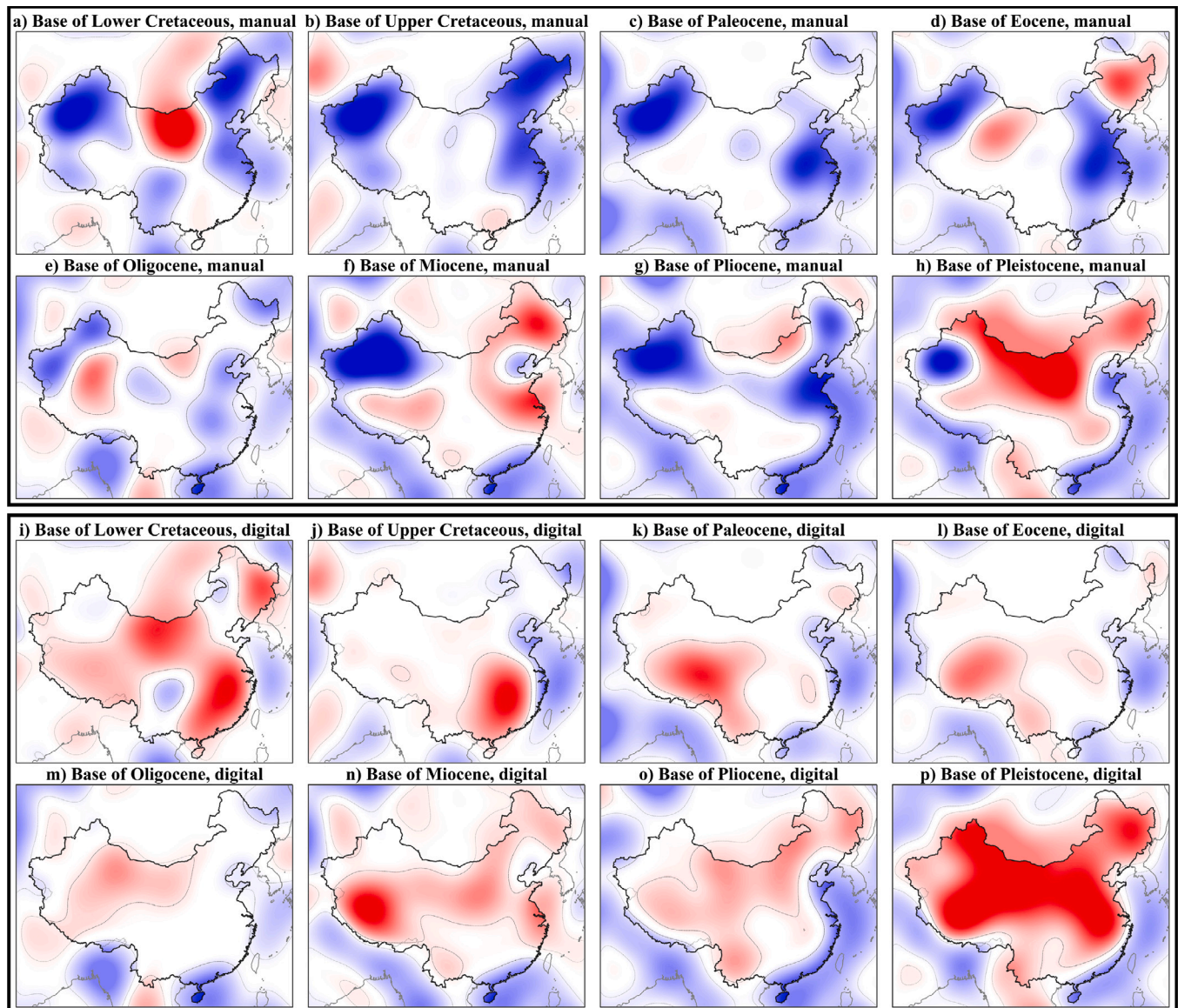


**Fig. 3.** Conformable and unconformable surfaces obtained after performing a spherical harmonic expansion of the data set in Fig. 2. Red indicates an unconformable surface while blue represents a conformable surface. The upper box are the surfaces obtained using the manual approach, while the lower box shows the surfaces for the digital approach. As in Fig. 2 surfaces inside of China are highlighted, while the ones outside China have less colour intensity. See Fig. 1 for projection and corner coordinates information.

approach (Fig. 3m) shows an unconformity. The Base of Miocene shows similar unconformable surfaces in both maps (Fig. 3f and n). Moreover, the manual approach depicts a conformable surface in the Tarim Basin whereas the digital approach shows a blank area. At the Base of Pliocene, we find another case where the two approaches show different behaviour in the same area. The manual approach (Fig. 3g) depicts a conformable surface traversing the country from east to west, whereas the digital approach (Fig. 3o) portrays an extensive unconformable surface extending from north to south. Finally, at the Base of Pleistocene, both approaches (Fig. 3h and p) coincide with an unconformable surface covering the country, with the exception of the west of the Tarim Basin, where the manual approach shows a conformity.

### 3.1.1. Rates

In order to facilitate the identification of the differences between the time-evolution of the un/conformable surfaces from one geological series to another, we present a visual comparison between the surfaces

of two successive maps (Fig. 4). We define a *persistent area* as an area that remains with the same behaviour, either conformable or unconformable, between two successive geological series. Conversely, we define an *evolving area* as an area that changes from conformable to unconformable or vice versa between two consecutive geological series. Areas that are white in either of the maps are classified as having *no information*, even if they show an un/conformity in one of the time windows. Blank areas indicate that no sedimentation of the *target* geological series occurred in those areas. Therefore when comparing two maps we cannot draw any inferences, because we do not know what happened to this area. Fig. 4 shows the persistent and evolving areas for the time range studied. Fig. 4a), for instance, depicts the evolution between the Base of Lower Cretaceous (Fig. 3a) and the Base of Upper Cretaceous (Fig. 3b) maps from the manual approach. The subplots in Fig. 4 show that areas evolving from unconformable to conformable or vice versa are relatively limited in China at the analysed length-scales, and over the course of the studied time range. The plots predominantly feature persistent areas or areas without sufficient information. In the



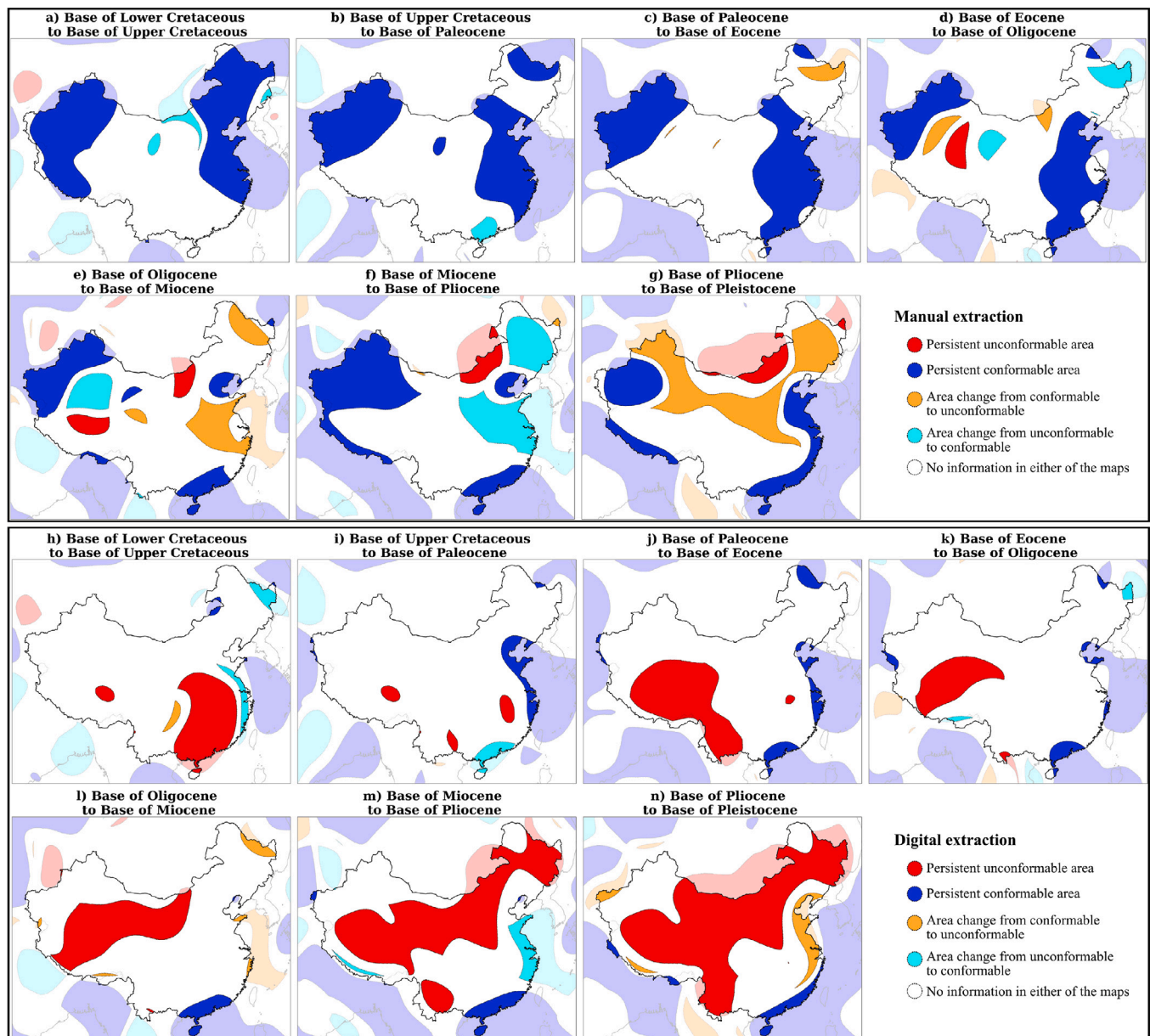


**Fig. 4.** Evolving and persistent un/conformable areas comparing two consecutive geological series for the manual approach (upper box) and the digital approach (lower box). Blue and red represent areas that remained conformable or unconformable, respectively. Evolving areas are shown in cyan where there was a change from unconformable to conformable and in orange for areas changing from conformable to unconformable. Blank surfaces are areas that there is not any information in either of the geological series involved. As with Figs. 2 and 3 the surfaces inside of China are highlighted, while the ones outside China have lower colour intensity. See Fig. 1 for projection and corner coordinates information.

manual approach, the western corner of the country appears to be consistently characterised by conformable contacts throughout the studied time period, see Figs. 4a–g. The Tarim Basin and the central-eastern regions of the country exhibit surfaces that change exclusively during the mid-late Cretaceous in the manual approach (Figs. 4e–g), for instance, in the map that shows the rates from the Base of Oligocene to the Base of Miocene (Fig. 4e). Similarly, the digital approach is characterised by the dominance of unconformable areas and white regions. There are minor evolving areas in the south-east of the country in the map that shows the rates from the Base of Lower Cretaceous to the Base of Upper Cretaceous (Fig. 4h). The rates from the Base of Pliocene to the Base of Pleistocene (Fig. 4n) also exhibits notable changes in both approaches. A quantitative analysis of the proportions of persistent and evolving area over time can be found in Fig. C.1 of the Appendix.

### 3.2. Hiatus ratio

In Fig. 5, we present hiatus ratio curves for both the manual and digital approaches, with the corresponding uncertainties as described in Section 2.5. It is evident that there is a significant discrepancy between the ratios derived from the digital and manual approaches. In the manual approach, the ratios tend to be lower than 50%, indicating a higher proportion of conformable areas in the maps (see Fig. 3a–h). Contrarily, the digital approach shows ratios typically higher than 70%, which is a consequence of the prevalence of the hiatus/unconformable areas in the majority of the maps (see Fig. 3i–p). The uncertainty for each approach is also included in shaded grey, showing variable range for the different series. As explained in Section 2.5, the uncertainty is derived with a maximum bound from considering the blank areas as either a conformable or an unconformable surface. It should be

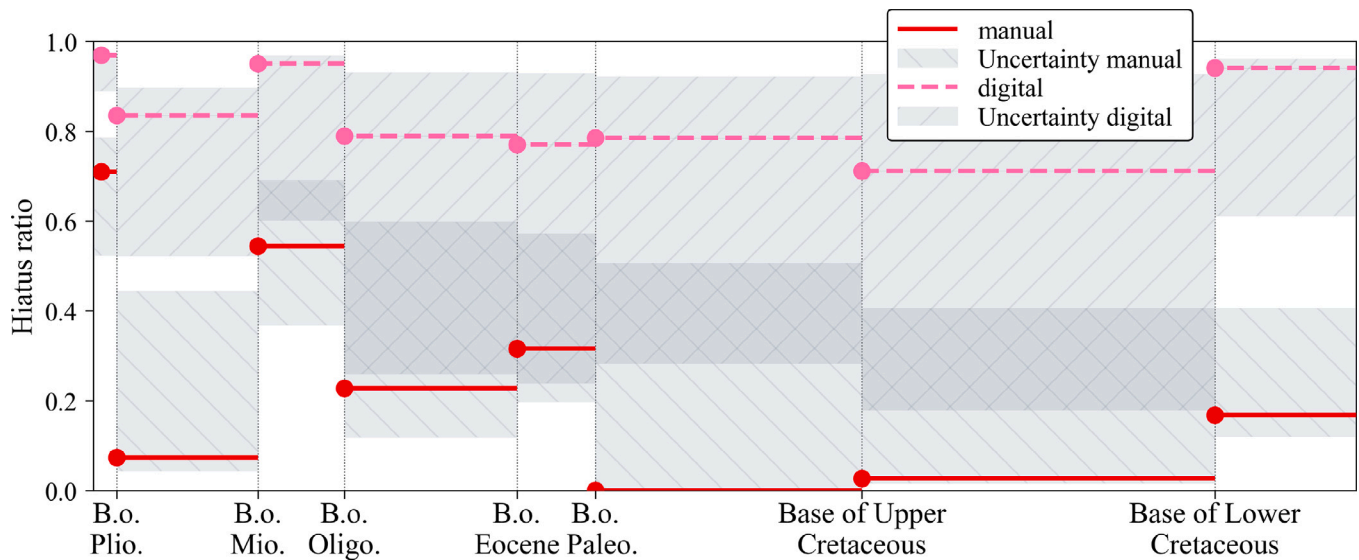


**Fig. 5.** Hiatus ratio (i.e., unconformable surface area divided by total unconformable+conformable area) of the conformable/unconformable surfaces from Fig. 3. Solid red/dashed pink lines mark the hiatus ratio for the manual/digital approaches, while the dots mark the datum. Uncertainty is plotted in grey with north-west-south-east pattern hatched for the manual approach and south-west-north-east hatched for the digital. B.o. indicates “Base of”. Only the surfaces within China are considered.

noted that the uncertainty is asymmetric for both approaches, with generally larger uncertainties towards the higher end of hiatus ratios for the manual extraction, and larger uncertainties towards smaller hiatus ratios for the digital approach. This is due to the fact that conformable areas typically dominate in the manual approach, whereas unconformable/hiatus areas are much more prominent in the digital approach. This is a consequence of the effect of filling the blank areas with the dominant signal (conformable for the manual approach and unconformable for the digital approach), which reduces the overall hiatus ratios, resulting in different behaviour for the manual and digital approaches.

The general trends of increase or decrease in the hiatus ratio from one series to the next, Fig. 5, are very similar for both approaches. They both show a decrease in the hiatus ratio between the Base of Lower Cretaceous and the Base of Upper Cretaceous. Similarly, this happens also for the younger series between the Base of Eocene and the Base of Pliocene, although the differences between the time ranges are more pronounced with the manual approach. Both approaches show an increase from the Base of Oligocene to the Base of Miocene, a decrease from the Base of Miocene to the Base of Pliocene and an increase afterwards from the Base of Pliocene to the Base of Pleistocene. In contrast, the relative increase of unconformable areas at the Base of Paleocene is noticeable with the manual approach but is not reproduced with the digital approach.

#### 4. Discussion

The use of the geological record to infer mantle processes has proved to be a highly valuable approach. Mapping hiatus surfaces at continental scale has provided us with a tool to observe and track the effects of mantle convection, particularly mantle plumes (Vibe et al., 2018b; Carena et al., 2019; Hayek et al., 2020, 2021; Vilacís et al., 2022; Stotz et al., 2024; Vilacís et al., 2024). In these publications, we followed the methodology introduced by Friedrich et al. (2018) and Friedrich (2019), and used a manual and a digital approach to extract stratigraphic hiatus. The approach used depended on the availability of digital data, the scale of the geological maps, and the online resources available. While the main goal was to map unconformable and conformable contacts, as well as the resulting hiatus surfaces, it should be noted that the processing steps and the assumptions made for each approach differ. Consequently, we performed in this study a comparative

analysis of the various methodologies that have been employed. We compared the extraction of unconformable and conformable contacts for the case of mainland China. For the manual approach, the contacts for Asia, including those in China, were extracted manually in a separate study (Vilacís et al., 2024), whereas in this study, we use the recent publication of the digital geological map of China (Pang et al., 2017), to process the map digitally, using the approach described in Section 2.3. It is important to note that given the dimensions of China, the comparison yields meaningful results, even though the mapping is not carried out on the scale of the continent. Furthermore, China is also sufficiently large for the spherical harmonic expansion we utilised to be sensitive to changes in the behaviour of the data, which is designed to emphasise mantle processes, and thereby highlights wavelengths larger than 1000 km (spherical harmonic degree smaller than 30). This is done to filter finer-scale tectonic features, including those from crustal flexure, compression or extension, and other erosional processes. These processes together with sea-level changes may create or induce, also, hiatus surfaces. We usually can disentangle them from mantle convection by observing mainly the large-scale patterns. However, it is possible that some upper mantle signals can also be present at smaller wavelengths as pointed out in Holdt et al. (2022). In the case of eustatic changes, we separate them from mantle signals by comparing different regions during the same time series: a global sea-level change will affect most continents similarly, while dynamic topography has a regional impact, as pointed out by Vilacís et al. (2024).

##### 4.1. Manual vs digital approach

The first comparison concerns the processing time. While the manual approach can require one or two weeks of continuous work to identify the studies and map all the contacts, the digital approach is considerably more time-efficient, with processing times reduced to just a few days. In the manual approach, the initial step is to compile a range of data sources, including regional studies, geological maps or on-line databases. Adding subsurface information may become a laborious process, depending on the accessibility of data and the complexity of locating the necessary material. For instance, the manual compilation of data for China took a few days, but for entire Asia it increased to several weeks. The process could be accelerated by the availability of a single geological map of Asia at geological series resolution. After

locating the data, another time-consuming step involves reading the studies, georeferencing and reprojecting the data. Following this, the contacts are manually mapped for each geological series within the specified time period. In contrast, the digital approach requires the utilisation of a digital geological map in a *GIS* format, the creation of a dictionary that maps age descriptions to their numerical value, and the subsequent digital processing. The most time-consuming aspect of this process, assuming that the digital geological map is already created, is the creation of the dictionary, as the nomenclature used to define age ranges is not standardised across countries or continents, with different approaches being used to describe them. The extraction of the points is relatively efficient and autonomous (see Section 2.1). However, to ensure a precise and equitable comparison, it would be necessary to only use the same single geological map for the manual and digital extraction, which is currently not possible. The primary challenge lies in the scarcity of digitised geological maps, which on itself is a processes that is notably time-consuming. Although some geological maps have been digitised in recent years, there is still a lack of them in the required temporal and spatial scales. For instance, Africa, one of the largest continents, currently lacks any digital map at a spatial scale larger than 1:10,000,000 and a temporal scale of geological series or stages.

A comparative analysis of the un/conformable points and surfaces reveals that the manual approach has considerably higher amounts of conformable information than the digital approach. This discrepancy can be attributed to the fact that the manual approach includes subsurface information, whereas the digital approach is limited to the outcrop data incorporated into the digital geological map. By definition, this leads to a lack of information below the datum horizon and results in the un/conformable maps displaying blank areas where there is no information of the *target* geological series in the geological maps, leading to large uncertainties (Friedrich, 2019). Furthermore, the digital approach is restricted to mapping areas where a contact between polygons is present. As a result, a basin delineated by a single polygon (e.g., the Tarim Basin) can only be mapped along its polygon border, with the centre of the basin showing as a blank area in the maps. The main advantage of the manual approach is that it allows for the incorporation of additional data and thus the reduction of said uncertainties (Carena et al., 2019). Moreover, the integration of subsurface information from sedimentary basins is crucial for the identification of subsurface rocks that may only be present in those basins.

In the case of China, the subsurface information used, particularly in the principal sedimentary basins, has a significant impact on the results, leading to a notable increase of conformable points in the maps. Fig. 6 shows the impact of removing the subsurface information from the Tarim, Junggar, Turfan, Qaidam, Minhe, Hexi, Songliao, North China, Hailar, Ordos and Middle Amur Basins on the hiatus ratio in the manual approach (red dotted line). The removal of this information is done digitally, where the points inside the outline of the basins (see the red lines in Fig. 1b) are removed. This removal results in a shift of the hiatus ratio towards higher values, representing a relative reduction of the conformable surface area. It is evident that the hiatus ratio for the manual approach is now much more closely aligned with the hiatus ratio derived from the digital approach, particularly during the Cenozoic. Moreover, adding extra information, especially in the form of subsurface information, contributes to a reduction in uncertainty. This is a limitation of the digital geological map, as the areas covered with young strata, such as Holocene sediments, remain blank throughout all time series studied.

Another reason for the increase of conformable points in the manual approach compared to the digital approach is how we map the contacts between geological series when the temporal resolution of the sediments is larger than geological series. Despite the fact that the input data is mainly in geological series, sometimes, the age description of a rock is given by a combination of geological series, systems or even

larger time intervals. In the manual approach we addressed this issue by assuming that if a rock is described by a geological system, the inner series of that system must also be present, thereby resulting in the addition of conformable contacts. In contrast, in the digital approach, the polygon is defined solely by an older and younger age boundary, as provided by the dictionary, without verification of whether the resolution of that polygon exceeds the temporal range of geological series. Consequently, in this approach, no contact between the inner series of the system is mapped, resulting in the area being left blank.

If we focus our attention only on the unconformable points, we see that their location is similar for both approaches (see Fig. 3). Furthermore, both approaches show a reduction of the amount of points at the Base of Paleocene and the Base of Eocene.

It is important to note that the discrepancy between the manual and digital approaches may also be attributed to the construction of the digital geological map and the specific geology of the region in question. Firstly, it should be acknowledged that geological maps for the same region can differ on two main grounds: the spatial scale and the interpretation of geological units. The scale of a map determines how much resolved it is, with fragmentary outcrops of a certain age being present at one scale but not at another. Additionally, the interpretation of geological units is influenced by the extent of a contact and the age of the rock. This can result in discrepancies in the age of a rock. For instance, a rock can be categorised as Miocene in one map and as Oligocene in another.

Secondly, the region we are studying can also affect the discrepancies between both approaches. In the case of this study, the northern part of China is characterised by the presence of basins with young strata on top, particularly Quaternary sediments (Carroll et al., 2010; Wang et al., 2014, highlighted in Fig. 1(b)). This specific geological setting leads to extensive blank areas in the maps that have been processed digitally. For example, the Tarim basin extends from east to west for a distance of 1000 km, thus in this area the digital approach does not show any points. On the other hand, the southern region of China is subjected to the influence of the Tibetan mountain range and orogenic tectonism as a result of the collision between the Indian plate and Eurasia (Dewey and Burke, 1973; Pan et al., 2012). This process results in the formation of a high frequency of unconformities (Miall, 2016). It should be noted that the Tibetan area, due to the lack of basins, was only mapped, in the manual approach, using two geological maps of scale 1:2,500,000 (Hwang et al., 2008), and 1:5,000,000 (Ghose et al., 1990), whereas in the digital approach the geological map has a scale of 1:1,000,000 (Pang et al., 2017). That means that in this region we only have a map-to-map comparison with different spatial scales. The digital map resolves between 2.5 and 5 times as many small features as the maps used in the manual approach. Thus if the outcrops are small and therefore not represented on these big scale maps, this leads to extended blank areas covering the south of the country, instead of showing a signal. To sum up, the choice of region, the available data and the scale of the digital geological maps may have an impact on the comparison.

Finally, an important point of comparison is the methodology utilised for the mapping process. The manual approach is inherently more subjective when mapping the contacts compared to the digital approach, due to the fact that in the digital approach, the extraction of the contacts is objective and reproducible. In the manual approach, and in the construction of geological maps, there are some subjective choices incorporated in interpreting the literature or observations, which come into play when connecting the individual outcrops. This means that a contact between two units that is not fully exposed requires a decision regarding its extent and connectivity with other points or line objects. For instance, a contact that is partially covered by a younger series can be easily traced, yet this allows for a subjective choice to be made regarding its exact extent. This subjective interpretation constitutes a fundamental aspect of the “geological interpretation”, and its interpretation varies between geologists. Consequently, this



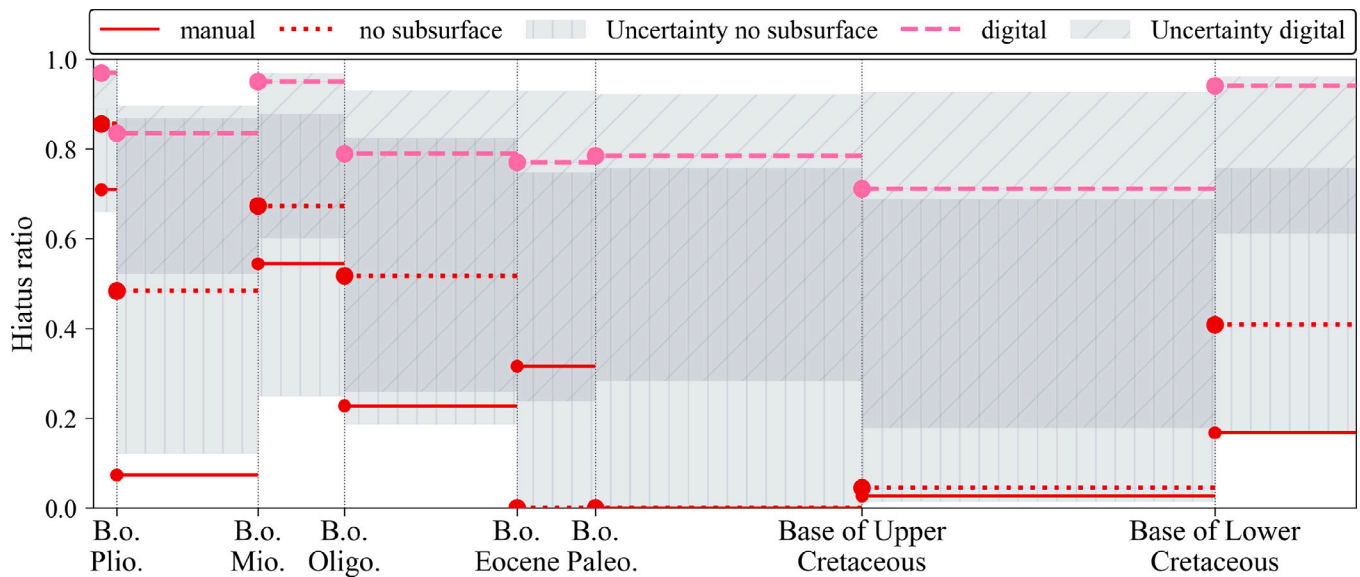


Fig. 6. As Fig. 5, hiatus ratio for the conformable/unconformable surfaces. In dashed red, we added, the ratio curve after removing the subsurface information of the basins from Fig. 1 in the manual approach. The uncertainty for this approach is shown in shaded grey and vertically hatched.

aspect must be given due consideration when selecting an approach. In the context of the digital approach, the subjectivity is inherent to the geological map itself; however, it is not further developed when extracting the contacts and allows for reproducibility and transparency of the final results.

#### 4.2. Hiatus maps

In our previous publications (Vibe et al., 2018b; Hayek et al., 2020, 2021; Stotz et al., 2021; Vilacís et al., 2022; Stotz et al., 2023, 2024; Vilacís et al., 2024) we used the so-called hiatus maps. These maps are obtained using the “hiatus/no hiatus” mapping described in Section 2.1. This mapping extracts the absence and presence (i.e., hiatus and no hiatus) of a specific geological series. The resulting maps represent the accumulation of processes that happened during that geological time series, and can be used as a proxy for dynamic topography. This mapping is different to the “Base of” mapping discussed so far, in which obtaining a proxy of dynamic topography for a single time unit necessitates the comparison of two consecutive maps. To illustrate this difference, in order to observe where Miocene sediments are present or absent with the “Base of” mapping, we need to examine the Base of Miocene map to determine where Miocene is present (coloured areas). We also need the Base of Pliocene map to identify where Miocene is absent (red surfaces). Contrarily, with the “hiatus/no hiatus” mapping, it is sufficient to analyse only the Miocene hiatus map to get the required information. Thus, these types of maps, the hiatus maps, provide a more direct link to the past dynamic topography of a region (see Hayek et al., 2020; Vilacís et al., 2024, for a comprehensive description), and they are preferred in geodynamics to observe mantle processes.

In Fig. 7, we show the hiatus/no hiatus surfaces and the associated hiatus ratio for China obtained using this alternative mapping choice. We show the results for the hybrid and digital approaches. The hybrid approach is a manual collection of the un/conformable contacts, followed by the digital incorporation of the occurrence of the preceding geological series. That means that to create the Miocene hiatus map, for instance, we add the points at the Base of Miocene as a no hiatus to the Base of Pliocene map, because they show the presence of Miocene. In contrast, the digital approach involves directly extracting the contacts from the digital geological map. The maps should be read and interpreted as follows: the Miocene hiatus maps (Fig. 7g and Fig. 7o), for instance, show the absence of Miocene sediments (*given* series) in red,

and serves as a proxy for uplift during that series. Conversely, the blue surfaces indicate the presence of Miocene sediments, and are used as a proxy for subsidence. The results change significantly when mapping the hiatus and no hiatus surfaces, i.e., the distribution (absence and presence) of a geological series, compared to the “Base of” mapping, which extracts unconformable and conformable contacts (see Fig. 3). In this case, both manual and digital approaches yield comparable hiatus maps, with the two hiatus ratio curves showing similar trends and falling within each other's uncertainties. Overall, there is also a reduction of the uncertainties, which can be attributed to the fact that this mapping choice incorporates more data, because we purposely add the occurrence of the *given* geological series (see in Section 2.1 the description of the “hiatus/no hiatus” mapping).

#### 4.3. Digital geological map analysis

Digital geological maps have a number of applications that extend beyond simply extracting hiatus. They are a new resource that facilitates the extraction of information in a more efficient manner. For example, it can be advantageous to quantify and extract the total area covered by a given base age, or to determine the number of polygons representing that base age (see Fig. 8). This type of quantification is important because the completeness of the stratigraphic record generally decreases with age, leading to potential under-representation of older conformable surfaces. This preservation bias may artificially inflate hiatus ratios in older time windows (i.e., Paleozoic or Precambrian). Although, the time range studied in this work should be less affected by this issue, we advise caution when interpreting data from before the Mesozoic, especially in regions with limited outcrop or subsurface data.

The number of amount of data in older ages affects the number of points in a un/conformable map, because it is directly related to the amount of points that form the polygons in the digital geological map, and the area that is covered by a base age. A high number of polygons with a younger base age, e.g., Quaternary sediments, reduces the amount of data that is extracted for older geological series. As illustrated in the upper plot of Fig. 8, the area covered by Quaternary (Holocene and Pleistocene) sediments is significantly larger (by a factor of three) compared to other base ages throughout the Phanerozoic and it is reduced by a factor of six in the Proterozoic. The bottom plot of Fig. 8 shows that the Base of Lower Cretaceous has almost double the number of polygons, yet they do not cover that much area. However,

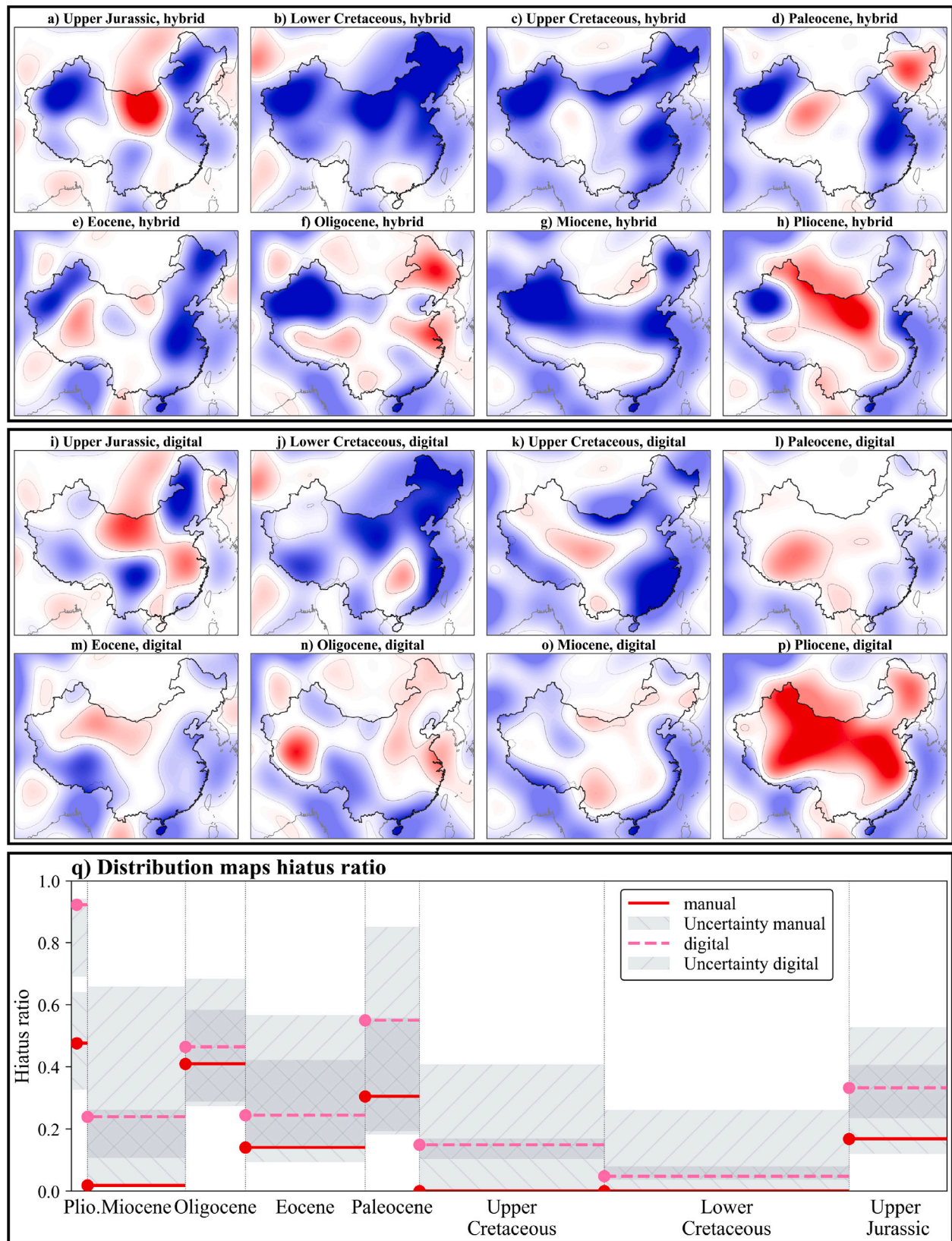


**Fig. 7.** Hiatus maps for China for the manual (upper box, a–h) and digital (lower box, i–p) extraction. Red and blue colours show the absence (hiatus) or occurrence (no hiatus) of a *target* geologic series since the Upper Jurassic. They serve as a proxy for the dynamic topography (red=high, blue=low) that the geological series has undergone. (q) Hiatus ratio for the hiatus maps (a–p) for the surfaces within China, with colours and patterns being the same as Fig. 5 and projection and coordinates as Fig. 1.

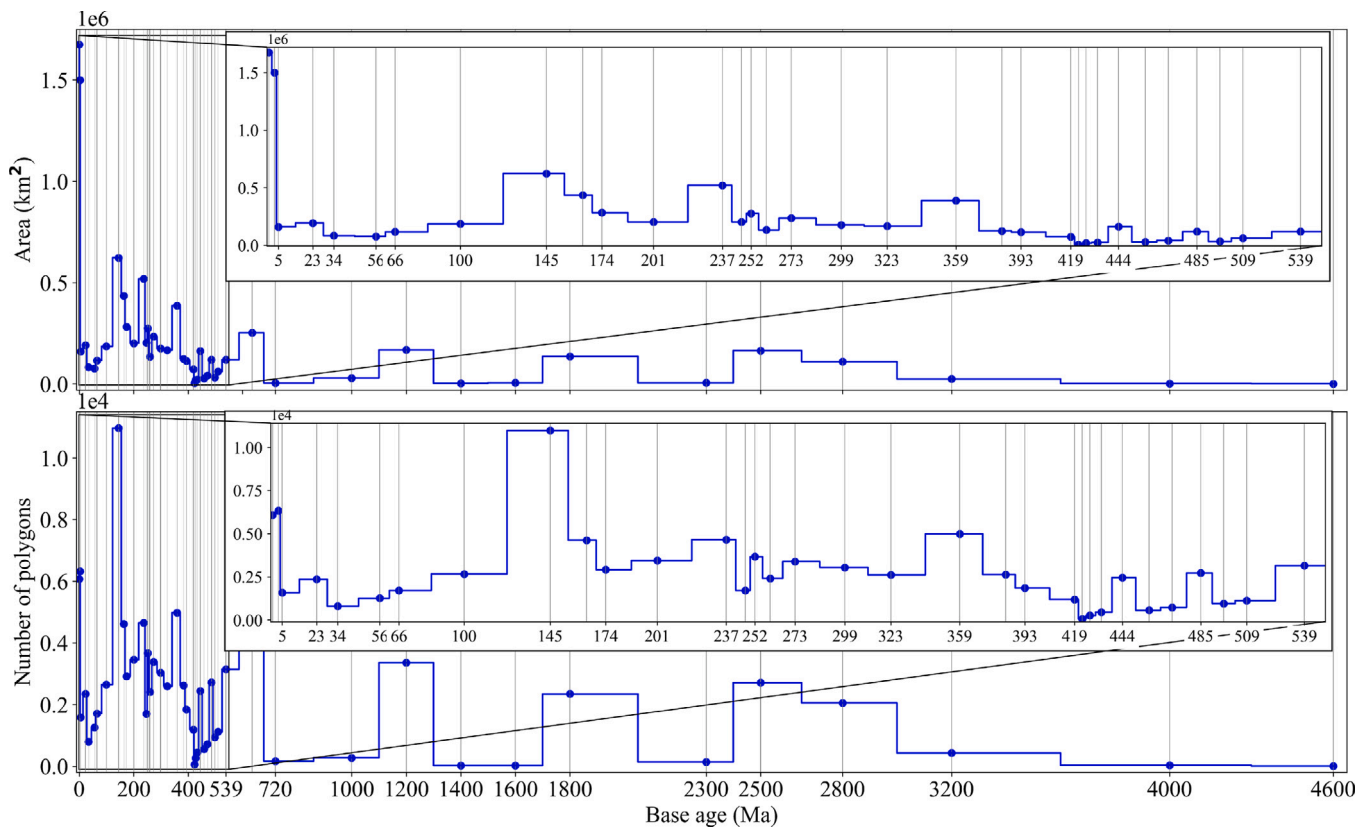


**Fig. 8.** Total area (top row) and number of polygons (bottom row) for a given base age in the digital geological map of China (Pang et al., 2017). Inset plots show the distribution curves during the Phanerozoic. The x-axis display the numerical base age of the polygon according to the chronostratigraphic chart of 2022 (Cohen et al., 2013) rounded to the nearest integer.

the amount of points extracted for this base age is going to be relatively larger than for the other base ages. A compilation of the areas of each polygon associated with a base age is depicted in Fig. D.1.

#### 4.4. Future geological maps

The creation of a geological map is a complex endeavour, with numerous decisions that need to be made at each stage of the process. As discussed in this manuscript, there are many factors in geological maps that indirectly affect the results of mapping hiatus surfaces. In the light of this, it is therefore imperative that geological maps are produced in a standardised manner at a global level, particularly in the context of the increased use of digital resources to process geological maps and their digitisation. These maps would be distinguished by their use of a standardised nomenclature for defining rock ages, a uniform time resolution, a common and well-referenced coordinate system and consistent spatial scales among other criteria. There are already important initiatives working towards unified and accessible geological data infrastructures, such as MacroStrat (Peters et al., 2018) and OneGeology (GSOs, 2007), which exemplify the importance of standardisation and open data framework at a global scale. Furthermore, the integration of geological maps that encompass both outcrop data and subsurface information would be advantageous (Şengör, 2016; Friedrich, 2019), as it would facilitate visualising older strata located beneath a young polygon, by simply removing the polygon.

The availability of these maps (in digital format and with subsurface information) would help to further explore and employ the geological data set as an observational tool to infer past dynamic processes. This data set that has been overlooked by these communities for a long time, because of the difficulties in visualising and integrating such data into computer models. The establishment of a unified digital

database, containing standardised maps, is proposed as a crucial step to foster enhanced transparency, facilitate research reproducibility and interdisciplinary collaborations, making the geological data set more widely accessible across other geoscience fields.

#### 5. Conclusions

Hiatus maps are a useful tool to observe and study past dynamic topographic patterns. In this work, we compared a manual and a digital approach to extract unconformable and conformable contacts between geological units, as well as the distribution of hiatus and no hiatus surfaces of a geological series. We performed this comparison for the case of China at the timescales of geological series, as this is the resolution of the digital geological map as well as our preexisting manual compilation. We find that the digital approach is more time-efficient, reducing the duration of data collection and processing from weeks to days. The results obtained from the manual and digital approaches show significantly different distributions of unconformable and conformable points when the “Base of” approach is used. This is due to the scale difference between the geological maps used in the digital and manual approaches, and to the fact that the digital approach is restricted to the outcrop data contained within the digital geological map, whereas the manual approach permits the utilisation of subsurface information. The latter, such as borehole data and stratigraphic columns, enriches mainly the conformable data set. In addition, introducing subsurface information results in a reduction of the amount of blank surfaces in the maps and consequently a reduction in uncertainties. The “hiatus/no hiatus” maps yield strikingly similar results between the hybrid and digital approach, demonstrating its robustness.

Our results indicate that the utilisation of digital processing of the data (when available) in conjunction with the incorporation of separate data sets (e.g., stratigraphic columns, drill cores, or regional



studies) mapped with the manual approach is the best approach. The primary benefit of automating the process, apart from being less time-consuming, is that it streamlines the manual process of interpreting map legends and select points, thereby enabling individuals to produce reliable hiatus maps, regardless of their expertise. This, in turn, would foster interdisciplinary collaborations and the utilisation of geological data as an observational tool. However, the lack of digital geological maps, and the fact that the ones that exist do not have uniform metadata or are standardised, represents a significant obstacle to using this data set. In conclusion, the establishment of a unified database containing standardised and fully digital geological maps is imperative to facilitate the integration of these diverse sources and to ensure the reliability and consistency of the resulting data.

### CRedit authorship contribution statement

**Berta Vilacís:** Writing – review & editing, Writing – original draft, Visualization, Software, Methodology, Investigation, Formal analysis, Data curation, Conceptualization. **Sara Carena:** Writing – review & editing, Methodology, Data curation. **Jorge N. Hayek:** Software. **Gabriel Robl:** Writing – review & editing. **Hans-Peter Bunge:** Writing – review & editing, Supervision, Funding acquisition, Conceptualization. **Jincheng Ma:** Resources.

### Funding sources

B.V. has been supported by the Deutsche Forschungsgemeinschaft (DFG, German Research Foundation), research training group 2698/1 (UPLIFT), project number 440512084, J.N.H. by the DFG project number BU2012/18-1 and G.R. by the DFG project number SCHU2914/5-2. The IT resources of the geophysics chair is funded by the DFG project number 518204048 titled “Major Research Instrumentation”.

### Declaration of competing interest

The authors declare that they have no known competing financial interests or personal relationships that could have appeared to influence the work reported in this paper.

### Acknowledgements

We would like to thank to Christian Heine, Gareth Roberts and Anke Friedrich for their thoughtful comments that helped improve the manuscript. Also, we would like to thank Shuang Liang for her work in converting the original files of the digital geological map of China (Pang et al., 2017) from *MapGIS* to a *shapefile* format.

## Appendix A. Digital extraction

### A.1. File preparation

To reproject the data to a standard global coordinate system, we developed and utilised a *Python* program that uses the *Shapely* library (Gillies et al., 2007–2025), *Scipy* library (Virtanen et al., 2020) and the *GeoPandas* (Jordahl et al., 2020) library and data structure. These libraries are employed to obtain a mapping relationship between the associated “GRID” files from each map and the global coordinates. We use a least squares approach, a statistical procedure to obtain the best the parameter mapping between the given and true coordinates for two geometrical raster transformations: one affine and one projective. The affine transformation is used for scaling, skewing and rotating the original map while preserving the parallelism and is defined as,

$$\begin{cases} x_{af} = ax + by + c \\ y_{af} = dx + ey + f \end{cases} \quad (3)$$

where  $a$ ,  $b$ ,  $c$ ,  $d$ ,  $e$  and,  $f$  are the affine transform parameters,  $x$  and  $y$  the original coordinates, and  $x_{af}$  and  $y_{af}$  the affine coordinates. Contrarily, the projective transformation is also used for scaling and skewing but it does not preserve parallelism, length or angle, and distorts the map. It is defined as

$$\begin{cases} x_{proj} = \frac{ax_{af} + by_{af} + c}{gx_{af} + hy_{af} + 1} \\ y_{proj} = \frac{dx_{af} + ey_{af} + f}{gx_{af} + hy_{af} + 1} \end{cases} \quad (4)$$

where  $a$ ,  $b$ ,  $c$ ,  $d$ ,  $e$ ,  $f$ ,  $g$  and  $h$  are the projective transform parameters, and  $x_{proj}$  and  $y_{proj}$  the new projective coordinates. The program is structured as follows:

1. Load the grid map and obtain the grid points corners of each map. Parallel to that, load the real coordinates that the corners must represent.
2. Find the affine transformation parameters using a least squares approach that gives the conversion from the original to the real coordinates.
3. Find the projective transform parameters using a least squares approach from the new affine coordinates to the real coordinates.
4. Apply the affine transform to the geological map.
5. Apply the projective transform to the geological map with the affine transform.
6. Change the crs projection to the geodetic coordinate system for the world (EPSG:4326).
7. Join all the maps together into a single shapefile and apply a 0.05 degrees northwards translation.

The resulting geological map of China is plotted in Fig. 1(a).

### A.2. Dictionary creation

This procedure uses the chronostratigraphic chart (Ogg et al., 2016), for which in this work we utilised the version of the chronostratigraphic chart from 2022 (Cohen et al., 2013). For example, a polygon with a Miocene age would be assigned the values of 5 and 23, respectively, for the upper and lower age bounds, if we have the case of a Miocene-Oligocene polygon, then the assigned values would be 5 and 34. In the case of the geological map of China, the aforementioned dictionary was created using the “CODE1”, “SYMBOL” and “UNITNAME” attribute columns that are contained in the digital geological map of China (Pang et al., 2017). The “CODE1” attribute is an integer number that represents a geological age or group of ages associated with a given polygon. The “SYMBOL” attribute denotes the symbol or group of characters associated with the geological code, while the “UNITNAME” attribute provides supplementary information on the geological age or formation of the specific polygon. Utilising these data, we map the “CODE1” numbers to the geological series, systems, eras, or a combination of series and systems, that they represent see Table A.1. In cases where higher temporal resolution is available, we downsample the temporal resolution to geological series for consistency across the domain.

### A.3. Contact extraction

The program that extracts the contact information identifies the contacts by checking which polygons share boundaries, and then classifying each contact as conformable or unconformable based on the upper age and lower age bounds of the polygons. Specifically, it compares the lower age bound of the main polygon to the upper age of the adjacent one. The classification logic is as follows:

1. If the ages are the same, the contact is classified as conformable.

**Table A.1**

Example of the dictionary generated for the geological map of China (Pang et al., 2017), where CODE1 and Symbol were provided in the attribute table of the shapefile. After the creation of the dictionary, the age value representatives of each polygon are added in the attribute table and used in the contact extraction.

CODE1	Symbol	Age	Series old	Series young	Lower age	Upper age
101300	N	Neogene	Miocene	Pliocene	23	3
101310	N2	Pliocene	Pliocene	Pliocene	5	3
101320	N1	Miocene	Miocene	Miocene	23	5
101400	E-N	Paleogene-Neogene	Paleocene	Pliocene	66	3
101410	E3-N	Oligocene-Neogene	Oligocene	Pliocene	34	3
101420	E3-N1	Oligocene-Miocene	Oligocene	Miocene	34	5
101430	E2-N1	Eocene-Miocene	Eocene	Miocene	56	5
101440	E-N	Paleogene-Miocene	Paleocene	Miocene	66	5
101500	E	Paleogene	Paleocene	Oligocene	66	23
101510	E3	Oligocene	Oligocene	Oligocene	34	23

2. If the lower age bound of the main polygon is younger than the upper age bound of the adjacent polygon, the contact is classified as unconformable.
3. If the lower age bound of the main polygon is older than the upper age bound of the adjacent polygon, it does not assign any contact at this stage. This contact will instead be processed when the adjacent polygon is evaluated as the main polygon.

It is important to note that if a polygon's age is defined only at system level (rather than at geological series level), the workflow does not assume the presence of intermediate series, and only maps the contacts at the upper and lower age bounds. After the contacts for a target series are classified, the points forming the contact lines are extracted for further processing.

#### Appendix B. Visual comparison between manual and digital maps

Fig. B.1 compares the unconformable and conformable surfaces derived from the manual and digital approaches. The figure highlights regions where both approaches coincide with the same signal (red/blue for unconformable/ conformable surfaces), where only one approach provides information (orange/cyan), and where they diverge (grey areas). Overall, the figure illustrates that most regions where both datasets provide coverage are consistent between the two approaches. Grey

areas are limited and mainly occur due to the introduction of subsurface information in the manual approach. This visual comparison reinforces the complementary nature of the two approaches discussed in the main text.

#### Appendix C. Rates

Fig. C.1 shows the quantitative analysis of the evolving and persistent areas between two different maps for the manual (upper plot) and digital (bottom plot) approaches. Overall, the plots show that the blank areas (the target series is not present on the input data) dominate the graph, showing values of above 50% in the manual approach and above 70% in the digital approach. In the manual approach we also observe that there are persistent conformable areas above 30% in the majority of the series. This behaviour has the consequence that the evolving areas are fairly small, particularly for the digital approach, where they are less than 5%.

#### Appendix D. Digital geological map statistics

In Fig. D.1, we plot the area of each polygon in the digital geological map as a function of the base age of that polygon. We observe that the Base of Holocene and Pleistocene have a large spread of polygons with

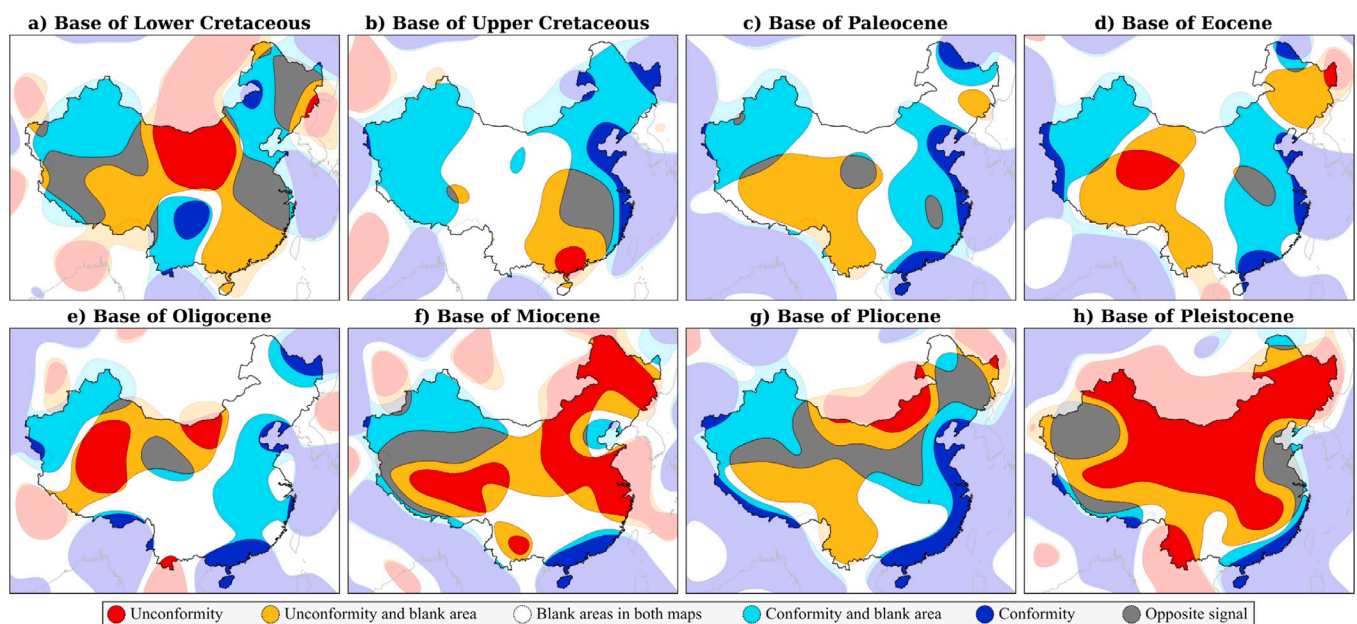


**Fig. B.1.** Comparison of the unconformable and conformable surfaces derived from the manual and digital approach. Red/blue means that both maps show an unconformable/conformable surface, orange/cyan means that one of them is unconformable/conformable and the other one does not provide any information, white means that both maps do not have any information, and grey indicates an opposite behaviour one of the approaches has a conformity and the other an unconformity.

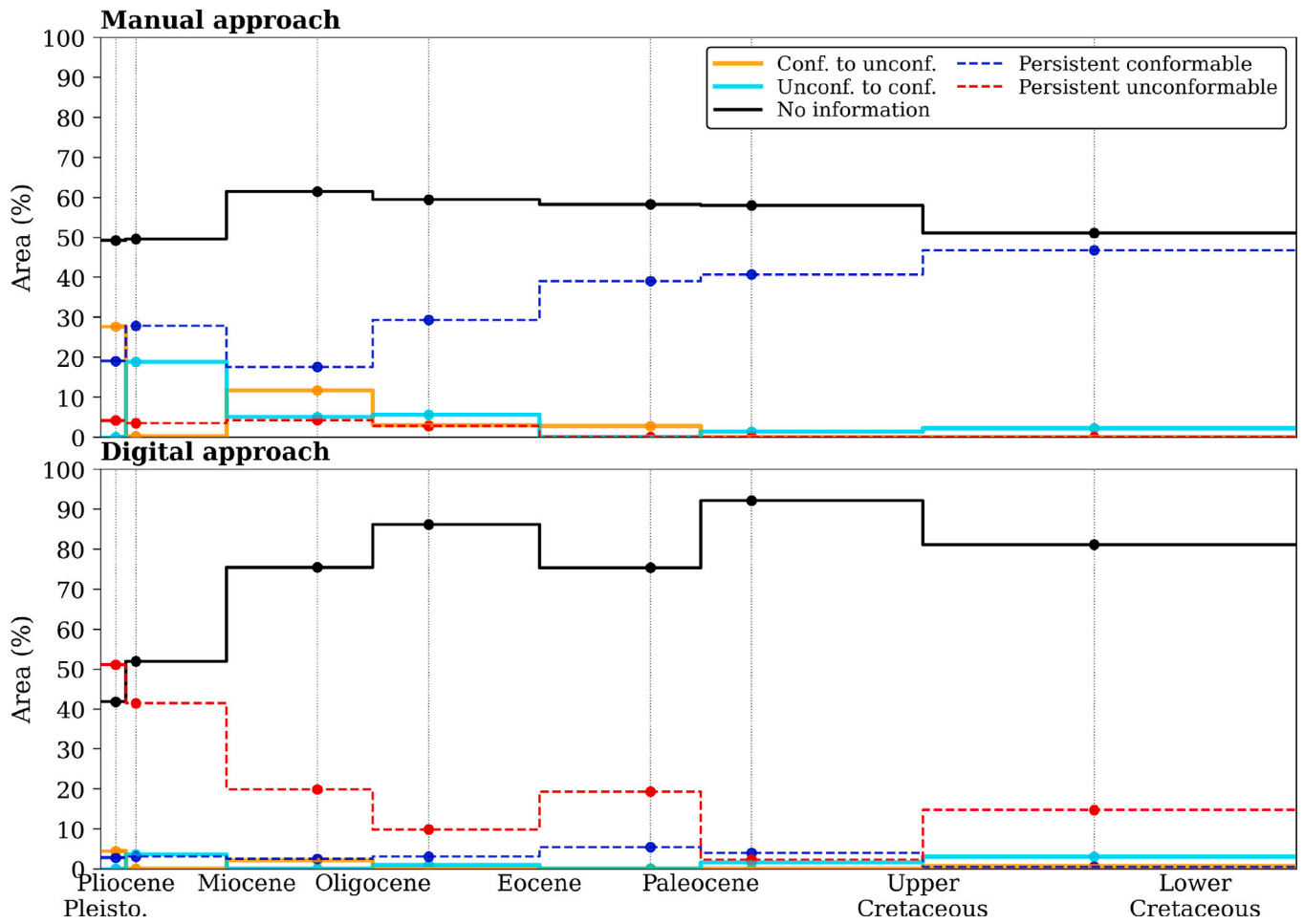


Fig. C.1. Calculation of evolving and persistent un/conformable surfaces from the Base of Lower Cretaceous to the Base of Pleistocene for the manual extraction (upper plot) and the digital extraction (lower plot). Cyan line represent the evolving areas from unconformable to conformable. Orange line represent the evolving areas from conformable to unconformable. Black lines are areas that do not have any information in either of the maps (they change from or to white or are consistently white). Finally, dashed-blue/red lines represent the persistent conformable and unconformable areas together, respectively.

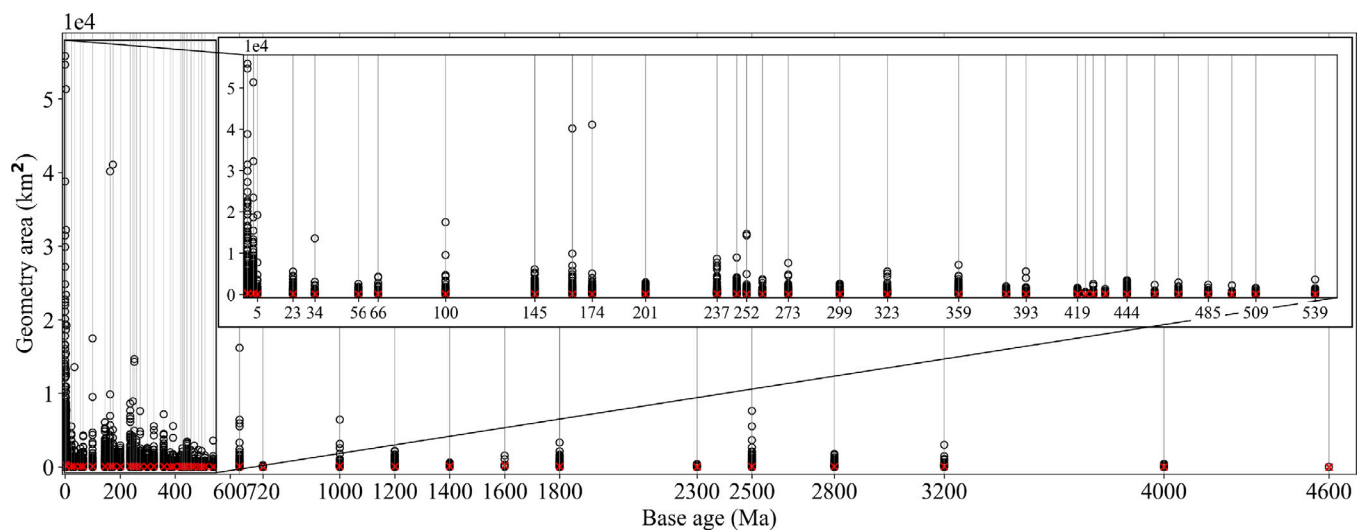


Fig. D.1. Area of each polygon (black circles) for a given base age that forms the digital geological map of China. Red cross shows the arithmetic mean area for each base age. As in Fig. 8, the x-axis display the numerical base age of the geometry according to the Chronostratigraphic chart of 2022 (Cohen et al., 2013) rounded to the nearest integer.



small and large areas, as visually shown in Fig. 1a. In contrast, polygons with base ages in the Proterozoic and Precambrian tend to have smaller areas, reflected the limited amount of geological data preserved from these older time intervals.

## Appendix E. Supplementary data

Supplementary material related to this article can be found online at <https://doi.org/10.1016/j.jsg.2025.105565>.

## Data availability

Data will be made available on request.

## References

- Barrell, J., 1917. Rhythms and the measurements of geologic time. *GSA Bull.* 28 (1), 745–904. <http://dx.doi.org/10.1130/GSAB-28-745>.
- Belousov, V.V., Maxwell, J.C., 1962. *Basic Problems in Geotectonics*. McGraw-Hill, New York, USA.
- Blackwelder, E., 1909. The valuation of unconformities. *J. Geol.* 17 (3), 289–299. [http://dx.doi.org/10.1130/0016-7606\(1963\)74\[93:SITCJO\]2.0.CO;2](http://dx.doi.org/10.1130/0016-7606(1963)74[93:SITCJO]2.0.CO;2).
- Bond, G.C., 1978a. Evidence for late Tertiary uplift of Africa relative to North America, South America, Australia and Europe. *J. Geol.* 86 (1), 47–65. <http://dx.doi.org/10.1086/649655>.
- Bond, G.C., 1978b. Speculations on real sea-level changes and vertical motions of continents at selected times in the Cretaceous and Tertiary Periods. *Geology* 6 (4), 247–250. [http://dx.doi.org/10.1130/0091-7613\(1978\)6<247:SORSICA>2.0.CO;2](http://dx.doi.org/10.1130/0091-7613(1978)6<247:SORSICA>2.0.CO;2).
- Bond, G.C., 1979. Evidence for some uplifts of large magnitude in continental platforms. *Tectonophysics* 61 (1–3), 285–305. [http://dx.doi.org/10.1016/0040-1951\(79\)90302-0](http://dx.doi.org/10.1016/0040-1951(79)90302-0).
- Brown, H., Colli, L., Bunge, H.P., 2022. Asthenospheric flow through the Izanagi-Pacific slab window and its influence on dynamic topography and intraplate volcanism in East Asia. *Front. Earth Sci.* 10, 10:889907. <http://dx.doi.org/10.3389/feart.2022.889907>.
- Burgess, P.M., Gurnis, M., Moresi, L., 1997. Formation of sequences in the cratonic interior of North America by interaction between mantle, eustatic, and stratigraphic processes. *Geol. Soc. Am. Bull.* 109 (12), 1515–1535. [http://dx.doi.org/10.1130/0016-7606\(1997\)109<1515:FOSITC>2.3.CO;2](http://dx.doi.org/10.1130/0016-7606(1997)109<1515:FOSITC>2.3.CO;2).
- Burke, K., Whiteman, A.J., 1973. Uplift, rifting and break-up of Africa. In: Tarling, D.H., Runcorn, S.K. (Eds.), *Implications of Continental Drift To the Earth Sciences*. Academic Press, London & New York, pp. 735–755.
- Campbell, I.H., 2007. Testing the plume theory. *Chem. Geol.* 241 (3–4), 153–176. <http://dx.doi.org/10.1016/j.chemgeo.2007.01.024>.
- Carena, S., Bunge, H.P., Friedrich, A.M., 2019. Analysis of geological hiatus surfaces across Africa in the Cenozoic and implications for the timescales of convectively-maintained topography. *Can. J. Earth Sci.* 56 (12), 1333–1346. <http://dx.doi.org/10.1139/cjes-2018-0329>.
- Carroll, A.R., Graham, S.A., Smith, M., 2010. Walled sedimentary basins of China. *Basin Res.* 22 (1), 17–32. <http://dx.doi.org/10.1111/j.1365-2117.2009.00458.x>.
- CGG-Robertson, 2022. Living atlas sedimentary basins of the world: Sedimentary basins of the world. <https://www.arcgis.com/home/item.html?id=a15e179c3b6a45ef94107353c2f64fc1>. (Last Accessed 10 December 2022).
- Cohen, K.M., Finney, S., Gibbard, P.L., Fan, J.X., 2013. The ICS international chronostratigraphic chart. *Episodes* 36 (3), 199–204. <http://dx.doi.org/10.18814/epiugs/2013/v36i3/002>, Version 2022/02.
- Cox, K., 1989. The role of mantle plumes in the development of continental drainage patterns. *Nature* 342 (6252), 873–877. <http://dx.doi.org/10.1038/342873a0>.
- Dewey, J.F., Burke, K.C.A., 1973. Tibetan, variscan, and precambrian basement reactivation: Products of continental collision. *J. Geol.* 81 (6), 683–692. <http://dx.doi.org/10.1086/627920>.
- Friedrich, A.M., 2019. Palaeogeological hiatus surface mapping: A tool to visualize vertical motion of the continents. *Geol. Mag.* 156 (2), 308–319. <http://dx.doi.org/10.1017/S0016756818000560>.
- Friedrich, A.M., Bunge, H.P., Rieger, S.M., Colli, L., Ghelichkhan, S., Nerlich, R., 2018. Stratigraphic framework for the plume mode of mantle convection and the analysis of interregional unconformities on geological maps. *Gondwana Res.* 53, 159–188. <http://dx.doi.org/10.1016/j.gr.2017.06.003>.
- Ghose, G., Chatterjee, D., Banerjee, J., 1990. *Geological map of south and east Asia*. Commission for the Geological Map of the World/UNESCO, third edition. scale 1:5 M, 6 sheets.
- Gillies, S., et al., 2007–2025. Shapely: Manipulation and analysis of geometric objects. URL <https://github.com/Toblerity/Shapely>. Version 2.0.4.
- GSOs, G., 2007. OneGeology - A Global Geoscience Data Platform. OneGeology Portal <https://onegeology.org>.
- Gurnis, M., 1998. Cretaceous Vertical Motion of Australia and the Australian–Antarctic Discordance. *Science* 279 (5356), 1499–1504. <http://dx.doi.org/10.1126/science.279.5356.1499>.
- Hager, B.H., Clayton, R.W., Richards, M.A., Comer, R.P., Dziewonski, A.M., 1985. Lower mantle heterogeneity, dynamic topography and the geoid. *Nature* 313 (6003), 541–545. <http://dx.doi.org/10.1038/313541a0>.
- Harrington, L., Zahirovic, S., Salles, T., Braz, C., Müller, R.D., 2019. Tectonic, geodynamic and surface process driving forces of Australia's paleogeography since the Jurassic. In: Keep, M., Moss, S. (Eds.), *The Sedimentary Basins of Western Australia V: Proceedings of the Petroleum Exploration Society of Australia Symposium*, Perth, WA, 2019. p. 29.
- Hayek, J.N., Vilacís, B., Bunge, H.P., Friedrich, A.M., Carena, S., Vibe, Y., 2020. Continent-scale hiatus maps for the Atlantic Realm and Australia since the upper Jurassic and links to mantle flow induced dynamic topography. *Proc. R. Soc. A: Math. Phys. Eng. Sci.* 476 (2242), 20200390. <http://dx.doi.org/10.1098/rspa.2020.0390>.
- Hayek, J.N., Vilacís, B., Bunge, H.P., Friedrich, A.M., Carena, S., Vibe, Y., 2021. Correction: Continent-scale Hiatus maps for the Atlantic Realm and Australia since the upper Jurassic and links to mantle flow-induced dynamic topography. *Proc. R. Soc. A: Math. Phys. Eng. Sci.* 477 (2251), 20210437. <http://dx.doi.org/10.1098/rspa.2021.0437>.
- Holdt, M.C., White, N.J., Stephenson, S.N., Conway-Jones, B.W., 2022. Densely sampled global dynamic topographic observations and their significance. *J. Geophys. Res.: Solid Earth* 127 (7), <http://dx.doi.org/10.1029/2022JB024391>, e2022JB024391.
- Hwang, J.H., Leonov, Y., Li, T., Petrov, O., Tomurtogoo, O., 2008. *Atlas of geological maps of central Asia and adjacent regions*. Geological Publishing House, scale 1:2.5 M, 9 sheets, Beijing, China.
- Jordahl, K., den Bossche, J.V., Fleischmann, M., Wasserman, J., McBride, J., Gerard, J., Tratner, J., Perry, M., Badaracco, A.G., Farmer, C., Hjelle, G.A., Snow, A.D., Cochran, M., Gillies, S., Culbertson, L., Bartos, M., Eubank, N., maxalbert, Bilogur, A., Rey, S., Ren, C., Arribas-Bel, D., Wasser, L., Wolf, L.J., Journois, M., Wilson, J., Greenhall, A., Holdgraf, C., Filipe, Leblanc, F., 2020. Geopandas/geopandas: v0.8.1. Zenodo <http://dx.doi.org/10.5281/zenodo.3946761>, Version 1.0.1.
- Levorsen, A.I., 1933. Studies in paleogeology. *AAPG Bull.* 17 (9), 1107–1132. <http://dx.doi.org/10.1306/3D932BA2-16B1-11D7-8645000102C1865D>.
- Miall, A.D., 2016. The valuation of unconformities. *Earth-Sci. Rev.* 163, 22–71. <http://dx.doi.org/10.1016/j.earscirev.2016.09.011>.
- Mitrovica, J.X., Beaumont, C., Jarvis, G.T., 1989. Tilting of continental interiors by the dynamical effects of subduction. *Tectonics* 8 (5), 1079–1094. <http://dx.doi.org/10.1029/TC008i005p01079>.
- Oeser, J., 2009. Entwicklung Integrierter IT-Infrastrukturen Für Die Simulation Komplexer Geophysikalischer Prozesse (Ph.D. thesis). Ludwig-Maximilians-Universität München, Fakultät für Geowissenschaften, <http://edoc.ub.uni-muenchen.de/9900/http://nbn-resolving.de/urn:nbn:de:bvb:19-99000>.
- Oeser, J., Bunge, H.P., Mohr, M., 2006. Cluster design in the earth sciences: TETHYS. In: Gerndt, M., Kranzlmüller, D. (Eds.), *High Performance Computing and Communications—Second International Conference, HPC 2006, Munich, Germany*. In: *Lecture Notes in Computer Science*, 4208, Springer, pp. 31–40. [http://dx.doi.org/10.1007/11847366\\_4](http://dx.doi.org/10.1007/11847366_4).
- Ogg, J.G., Ogg, G.M., Gradstein, F.M., 2016. 1-Introduction. In: Ogg, J.G., Ogg, G.M., Gradstein, F.M. (Eds.), *A Concise Geologic Time Scale*. Elsevier, pp. 1–8. <http://dx.doi.org/10.1016/B978-0-444-59467-9.00001-7>.
- Pan, G., Wang, L., Li, R., Yuan, S., Ji, W., Yin, F., Zhang, W., Wang, B., 2012. Tectonic evolution of the Qinghai-Tibet Plateau. *J. Asian Earth Sci.* 53, 3–14. <http://dx.doi.org/10.1016/j.jseas.2011.12.018>, The Tibetan Orogenic Evolution: Pre- to Post-Collisional Geologic Records.
- Pang, J., Ding, X., Han, K., Zeng, Y., Chen, A., Zhang, Y., Zhang, Q., Yao, D., 2017. 1:1000000 spatial database of digital geological maps of the People's Republic of China. <http://dx.doi.org/10.23650/DATA.H.2017.NGA105570.T1.64.1>.
- Peters, S.E., Husson, J.M., Czaplewski, J., 2018. Macrostrat: A platform for geological data integration and deep-time earth crust research. *Geochim. Geophys. Geosystems* 19 (4), 1393–1409. <http://dx.doi.org/10.1029/2018GC007467>.
- Rainbird, R.H., Ernst, R.E., 2001. The sedimentary record of mantle-plume uplift. *Spec. Papers-Geological Soc. Am.* 352, 227–246. <http://dx.doi.org/10.1130/0-8137-2352-3.227>.
- Sahagian, D., 1987. Epeirogeny and eustatic sea level changes as inferred from cretaceous shoreline deposits: Applications to the central and western United States. *J. Geophys. Res.: Solid Earth* 92 (B6), 4895–4904. <http://dx.doi.org/10.1029/JB092i06p04895>.
- Sahagian, D., Jones, M., 1993. Quantified middle Jurassic to paleocene eustatic variations based on Russian platform stratigraphy: Stage level resolution. *GSA Bull.* 105 (8), 1109–1118. [http://dx.doi.org/10.1130/0016-7606\(1993\)105<1109:QMJTPE>2.3.CO;2](http://dx.doi.org/10.1130/0016-7606(1993)105<1109:QMJTPE>2.3.CO;2).
- Saunders, A., Jones, S., Morgan, L., Pierce, K., Widdowson, M., Xu, Y., 2007. Regional uplift associated with continental large igneous provinces: The roles of mantle plumes and the lithosphere. *Chem. Geol.* 241 (3), 282–318. <http://dx.doi.org/10.1016/j.chemgeo.2007.01.017>.

- Şengör, A.M.C., 2001. Elevation as indicator of mantle-plume activity. In: Ernst, R.E., Buchan, K.L. (Eds.), *Mantle Plumes: Their Identification Through Time*. Geological Society of America, pp. 183–245. <http://dx.doi.org/10.1130/0-8137-2352-3.183>, Volume 352.
- Şengör, A.M.C., 2003. The Large Wavelength Deformations of the Lithosphere: Materials for a History of the Evolution of Thought from the Earliest Times to Plate Tectonics. Geological Society of America, Memoir no. 196, p. 347. <http://dx.doi.org/10.1130/978-0-8137-1196-7-196.0.1>.
- Şengör, A.M.C., 2016. What is the use of the history of geology to a practicing geologist? The propaedeutical case of stratigraphy. *J. Geol.* 124 (6), 643–698. <http://dx.doi.org/10.1086/688609>.
- Sloss, L.L., 1963. Sequences in the Cratonic Interior of North America. *Geol. Soc. Am. Bull.* 74 (2), 93–114. [http://dx.doi.org/10.1130/0016-7606\(1963\)74\[93:STCIOJ2.0.CO;2](http://dx.doi.org/10.1130/0016-7606(1963)74[93:STCIOJ2.0.CO;2).
- Sloss, L.L., 1992. Tectonic episodes of cratons: Conflicting North American concepts. *Terra Nova* 4 (3), 320–328. <http://dx.doi.org/10.1111/j.1365-3121.1992.tb00821.x>.
- Stacey, F.D., Davis, P.M., 2008. *Physics of the Earth*. Cambridge University Press, New York, USA. <http://dx.doi.org/10.1017/CBO9780511812910>.
- Stille, H., 1924. Grundfragen der Vergleichenden Tektonik. *Gebrüder Borntraeger* 71, 1–443. <http://dx.doi.org/10.1017/S0016756818000560>.
- Stotz, I.L., Carena, S., Vilacís, B., Hayek, J.N., Bunge, H.-P., 2024. Kerguelen plume drives the eocene directional change in Australian plate motion. *Lithosphere* 2024 (3), [http://dx.doi.org/10.2113/2024/lithosphere\\_2023\\_289](http://dx.doi.org/10.2113/2024/lithosphere_2023_289), lithosphere\_2023\_289.
- Stotz, I.L., Vilacís, B., Hayek, J.N., Bunge, H.-P., Friedrich, A.M., 2021. Yellowstone plume drives neogene North American plate motion change. *Geophys. Res. Lett.* 48 (18), <http://dx.doi.org/10.1029/2021GL095079>, e2021GL095079.
- Stotz, I.L., Vilacís, B., Hayek, J.N., Carena, S., Bunge, H.-P., 2023. Plume driven plate motion changes: New insights from the south atlantic realm. *J. South Am. Earth Sci.* 124, 104257. <http://dx.doi.org/10.1016/j.jsames.2023.104257>.
- Suess, E., 1883. *Das Antlitz der Erde: Erster Band*. F. Tempsky, Prag und Wien, and G. Freytag, Leipzig.
- Vail, P.R., Mitchum Jr, R.M., Thompson III, S., 1977. Seismic stratigraphy and global changes of sea level: Part 4. Global cycles of relative changes of sea level: Section 2. Application of seismic reflection configuration to stratigraphic interpretation. In: *Seismic Stratigraphy: Applications To Hydrocarbon Exploration*. American Association of Petroleum Geologists, Memoir no. 26, pp. 83–97.
- Vibe, Y., Friedrich, A.M., Bunge, H.P., Clark, S.R., 2018b. Correlations of oceanic spreading rates and hiatus surface area in the North Atlantic realm. *Lithosphere* 10 (5), 677–684. <http://dx.doi.org/10.1130/L736.1>.
- Vilacís, B., Brown, H., Bunge, H.-P., Carena, S., Hayek, J.N., Stotz, I.L., Wang, R.Z., Friedrich, A.M., 2024. Dynamic topography and the planform of mantle convection since the jurassic inferred from global continental hiatus maps. *Proc. R. Soc. A: Math. Phys. Eng. Sci.* 480 (2302), 20240311. <http://dx.doi.org/10.1098/rspa.2024.0311>, Special feature: Foundations of Operational Geodynamics.
- Vilacís, B., Hayek, J.N., Stotz, I.L., Bunge, H.P., Friedrich, A.M., Carena, S., Clark, S., 2022. Evidence for active upper mantle flow in the atlantic and indo-Australian realms since the upper jurassic from hiatus maps and spreading rate changes. *Proc. R. Soc. A: Math. Phys. Eng. Sci.* 478 (2262), 20210764. <http://dx.doi.org/10.1098/rspa.2021.0764>.
- Virtanen, P., Gommers, R., Oliphant, T.E., Haberland, M., Reddy, T., Cournapeau, D., Burovski, E., Peterson, P., Weckesser, W., Bright, J., van der Walt, S.J., Brett, M., Wilson, J., Millman, K.J., Mayorov, N., Nelson, A.R.J., Jones, E., Kern, R., Larson, E., Carey, C.J., Polat, İ., Feng, Y., Moore, E.W., VanderPlas, J., Laxalde, D., Perktold, J., Cimrman, R., Henriksen, I., Quintero, E.A., Harris, C.R., Archibald, A.M., Ribeiro, A.H., Pedregosa, F., van Mulbregt, P., SciPy 1.0 Contributors, 2020. SciPy 1.0: Fundamental Algorithms for Scientific Computing in Python. *Nature Methods* 17, 261–272. <http://dx.doi.org/10.1038/s41592-019-0686-2>, Version 1.14.0.
- Wang, P., Li, Q., Li, C.F., 2014. Chapter 5 - basins and stratigraphy. In: Wang, P., Li, Q., Li, C.-F. (Eds.), *Geology of the China Seas*. In: *Developments in Marine Geology*, vol. 6, Elsevier, pp. 341–468. <http://dx.doi.org/10.1016/B978-0-444-59388-7.00005-6>.
- Watts, A.B., Moore, J.D.P., 2017. Flexural isostasy: Constraints from gravity and topography power spectra. *J. Geophys. Res.: Solid Earth* 122 (10), 8417–8430. <http://dx.doi.org/10.1002/2017JB014571>.
- Wheeler, H.E., 1958. Time-stratigraphy. *AAPG Bull.* 42 (5), 1047–1063. <http://dx.doi.org/10.1306/0BDA5AF2-16BD-11D7-8645000102C1865D>.
- Wieczorek, M.A., Meschede, M., 2018. Shtools: Tools for working with spherical harmonics. *Geochem. Geophys. Geosystems* 19 (8), 2574–2592. <http://dx.doi.org/10.1029/2018GC007529>.